

Using a modified version of the Tavis-Cummings-Hubbard model to simulate the formation of a neutral hydrogen molecule

Miao Hui-hui

Faculty CMC of Lomonosov Moscow State University

Ozhigov Yuri Igorevich*

Faculty CMC of Lomonosov Moscow State University

Valiev Institute of Physics and Technology of Russian Academy of Science

(Dated: February 6, 2023)

A finite-dimensional chemistry model with two two-level artificial atoms on quantum dots positioned in optical cavities, called the association-dissociation model of neutral hydrogen molecule, is described. The initial circumstances that led to the formation of the synthetic neutral hydrogen molecule are explained. In quantum form, nuclei's mobility is portrayed. The association of atoms in the molecule is simulated through a quantum master equation, incorporating hybridization of atomic orbitals into molecular - depending on the position of the nuclei. Consideration is also given to electron spin transitions. Investigated are the effects of temperature variation of various photonic modes on quantum evolution and neutral hydrogen molecule formation. Finally, a more precise model including covalent bond and simple harmonic oscillator (phonon) is proposed.

Keywords: neutral hydrogen molecule, artificial atom, finite-dimensional quantum electrodynamics, temperature variation, phonon.

I. INTRODUCTION

The ability of supercomputers to simulate restricted molecular structures within the framework of "quantum chemistry" — stationary states of molecules, has increased interest in mathematical modelling of natural phenomena, particularly predictive modelling of chemistry. This interest has recently been sparked by various theoretical papers, including those by [1–3]. Even before the construction of the full-scale quantum computer [2], quantum approaches open new perspectives for effectively modelling well-known effects and witnessing fundamentally novel phenomena in chemistry, compared to classical approaches. The modelling of hydrogen-related chemical reactions, particularly the formation and decomposition (reactions of association and dissociation, respectively) of the cation H_2^+ and neutral hydrogen molecule H_2 , is one of the main objectives of chemical modelling. The construction of large molecular structures, notably biomacromolecules like proteins and deoxyribonucleic acid, necessitates an understanding of hydrogen chemical processes. In works [4, 5], a thorough simulation of association and dissociation of the cation H_2^+ is put forward. Additionally, research has also been done on another work about the positive hydrogen peroxide ion OH^+ in a thermal bath [6]. The association reaction of the neutral hydrogen molecule H_2 in open Markovian systems is the focus of this paper.

The quantum electrodynamics (QED) model, which presents a distinct physical paradigm for examining interaction between light and matter, is a fundamental contribution to this paper. In this paradigm, fields (of cavities

are related to impurity two- or multi-level systems, which are typically referred to as atoms. We must utilize models resembling finite dimensional cavity QED models for "dynamical chemistry" because the description of the field is the major area of difficulty. The ultrastrong-coupling [7–11] (USC) of light and matter (e.g., a cavity mode and a natural or artificial atom, respectively) occurs when their coupling strength g becomes comparable to the atomic (ω_a) or cavity (ω_c) frequencies. More specifically, the USC regime occurs when $\eta = \max(\frac{g}{\hbar\omega_c}, \frac{g}{\hbar\omega_a})$ is within the range [0.1, 1). The quantum Rabi model (QRM) [12, 13] is the fundamental model for USC of a single two-level atom in a single-mode cavity. The Dicke [14] and Hopfield [15] models are two examples of its multi-atom or multi-mode generalizations. Deep strong coupling (DSC) is a common term used to describe the regime $\eta \geq 1$ [16]. The more straightforward strong coupling (SC) model — Jaynes-Cummings model (JCM) [17] can be used to replace these models for USC when $\eta < 0.1$. The JCM depicts the dynamics of a two-level atom in an optical cavity, interacting with a single-mode field inside it. Its generalization — the Tavis-Cummings model (TCM) [18] depicts the dynamics of a collection of N two-level atoms in an optical cavity. The Jaynes-Cummings-Hubbard model (JCHM) and Tavis-Cummings-Hubbard model (TCHM) [19] are generalizations of the JCM and TCM to multiple cavities coupled by an optical fibre. Due to the fact that SC is often simpler to realize in an experiment than USC and DSC, we modified these SC models in this paper to fulfil the needs of chemical reaction simulation. As finite-dimensional QED models, these models and their modifications are valuable because they enable us to describe a very complex interaction between light and matter. Among these models, the optical cavity — Fabry-Pérot resonator is the most

* Email address: ozhigov@cs.msu.ru

significant form, where atoms are held in place by optical tweezers. Many studies have been conducted recently in the field of JCM and its modifications, including those on phase transitions [20, 21], the search for metamaterials [22], quantum many-body phenomena [23], the realization of Grover search algorithm [24], quantum gates [25, 26], dark states [27–29], and other works [30, 32].

In this paper, we discuss modifications of finite-dimensional QED models that allow us to interpret chemical reactions in terms of artificial atoms and molecules on quantum dots positioned inside optical cavities. Between the cavities, quantum motion of nuclei is permissible. Association reaction differ only in the initial states. By using the Lindblad operators of photon leakage from the cavity to the external environment to solve the single quantum master equation (QME), chemical processes with two-level atoms are schematically described. QME approach has been used to examine the dynamics of

quantum open system [34], and it is consistent with the principles of quantum thermodynamics [35, 36]. Only Markovian approximations are applicable.

This paper is organized as follows. After introducing the association-dissociation model of the neutral hydrogen molecule in Sec. II, describing hybridization and dehybridization of a couple of two-level artificial atoms, and based on the TCHM [19], we introduce electron spin-flip in Sec. III. We also take into account how temperature changes in photonic modes affect quantum evolution and the formation of neutral hydrogen molecules in Sec. IV. In Sec. V, a more accurate model incorporating a phonon and a covalent bond is raised. We offer a numerical technique to achieve complexity reduction in Sec. VI. We present the results of our numerical simulations in Sec. VII. Some brief comments on our results and extension to future work in Sec. VIII close out the paper.

TABLE I: List of abbreviations and notations used in this paper.

Abbreviations/Notations	Descriptions
QED	Quantum electrodynamics
SC	Strong coupling
USC	Ultrastrong-coupling
DSC	Deep strong coupling
QRM	Quantum Rabi model
JCM	Jaynes-Cummings model
TCM	Tavis-Cummings model
JCHM	Jaynes-Cummings-Hubbard model
TCHM	Tavis-Cummings-Hubbard model
QME	Quantum master equation
RWA	Rotating wave approximation
AO	Atomic orbital
MO	Molecular orbital
<i>ph</i>	Photon
<i>e</i>	Electron
<i>at</i>	Atom
<i>or</i>	Orbital
<i>n</i>	Nucleus
<i>s</i>	Spin
\uparrow	Spin up
\downarrow	Spin down
<i>cb</i>	Covalent bond
Φ_0	Bonding orbital or molecular ground orbital
Φ_1	Antibonding orbital or molecular excited orbital
η	Maximum ratio of coupling strength to frequency
ω_c	Cavity frequency or photonic mode
ω_n	Transition frequency, including in molecular (or as ω) and in atom (or as Ω)
ω	Transition frequency for electron in molecule (e.g. ω^\uparrow , ω^\downarrow)
ω^\uparrow	Transition frequency for electron with \uparrow in molecule
ω^\downarrow	Transition frequency for electron with \downarrow in molecule
Ω or ω_a	Transition frequency for electron in atom (e.g. Ω^\uparrow , Ω^\downarrow)
Ω^\uparrow	Transition frequency for electron with \uparrow in atom
Ω^\downarrow	Transition frequency for electron with \downarrow in atom
Ω^s	Electron spin transition frequency in atom
Ω^c	Phonon mode
\mathcal{C}	Space of quantum states for entire system
\mathcal{A}	Subspace of quantum states for associative system (or molecular system)
\mathcal{D}	Subspace of quantum states for dissociative system (or atomic system)
ρ	Density Matrix

Continued on next page

— continued from previous page

Abbreviations/Notations	Descriptions
$\mathcal{L}(\rho)$	Lindblad superoperator
\mathcal{K}	Graph of the potential photon dissipations between the states that are permitted
\mathcal{K}'	Graph of potential photon influxes that are permitted
$L_k(\rho)$	Standard dissipation superoperator
$L_{k'}(\rho)$	Standard influx superoperator
γ_k	Total spontaneous emission rate for photon
$\gamma_{k'}$	Total spontaneous influx rate for photon
μ	Ratio of influx rate to emission rate (e.g. μ_ω , μ_Ω , μ_{Ω^s})
A_k	Lindblad or jump operator of system and its hermitian conjugate operator — A_k^\dagger
H	Hamiltonian
\hbar	Reduced Planck constant or Dirac constant
a	Photon annihilation operator (e.g. a_ω , a_Ω , a_{Ω^s}) and its hermitian conjugate operator — a^\dagger
σ	Interaction operator of atom with the electromagnetic field of the cavity (e.g. σ_ω , σ_Ω , σ_{Ω^s} , σ_n) and its hermitian conjugate operator — σ^\dagger
g or g_n	Coupling strength of photon and the electron (e.g. g_ω , g_Ω)
ζ	Nucleus tunnelling strength or atom leap strength (e.g. ζ_0 , ζ_1 , ζ_2)
$\mathcal{G}(T)_f$	Thermally stationary state
K	Boltzmann constant
T	Temperature for photonic mode (e.g. T_ω , T_Ω , T_{Ω^s})
c	Normalization factors (e.g. c_0 , c_1 , c_2 , c_3)
V	Effective volume of the cavity
d	Dipole moment of the transition between the ground and the perturbed states
$E(x)$	Spatial arrangement of the atom in the cavity
l	Length of the cavity
λ	Photon wavelength
N	Number of atoms
M	Number of cavities
I_a	Unit operator
I_σ	Unit operator

II. THE ASSOCIATION-DISSOCIATION MODEL OF NEUTRAL HYDROGEN MOLECULE

The association-dissociation model of the neutral hydrogen molecule is modified from the TCHM (see Appx. A). In this model, each energy level, both atomic and molecular, is split into two levels with the same energy (approximately the same, with accuracy to Stark splitting): spin up and spin down, which are indicated by the signs \uparrow and \downarrow , respectively. To differentiate each level on the spin, we will add these marks that indicate the energy level. Now the levels will be twice as much, and for each level there must be no more than one electron according to Pauli exclusion principle [37]. Thus, photons that excite the electron will be of the same type as the chosen spin direction.

Hybridization of atomic orbitals (AO) and formation of molecular orbitals (MO) are shown in Fig. 1(a) and Fig. 1(b), where bonding orbital takes the form $\Phi_0 = 1/\sqrt{2}(0_1 + 0_2)$ and antibonding orbital takes the form $\Phi_1 = 1/\sqrt{2}(0_1 - 0_2)$. The electrons will be bound in the potential wells that each nucleus creates around itself. Fig. 1(c) displays the association reaction of H_2 . Two electrons in the atomic ground orbital -1 with significant gaps between their nuclei, which correspond to two distinct spin directions, absorb respectively photons with modes Ω^\uparrow or Ω^\downarrow , before rising to the atomic excited orbital 0 . The potential barrier between the two

potential wells decreases when nuclei from different cavities come together in one cavity due to the quantum tunnelling effect. Since the two electrons are in atomic excited orbitals, the atomic orbitals are hybridized into molecular excited orbitals, and the electrons are released on the molecular excited orbital Φ_1 . Then, two electrons quickly emit photons with the modes ω^\uparrow or ω^\downarrow , respectively, and fall to the molecular ground orbital Φ_0 . Stable molecule is formed. Fig. 1(d) depicts the dissociation reaction of H_2 . Two electrons in the molecular ground orbital absorb respectively photon with modes ω^\uparrow or ω^\downarrow , rising to the molecular excited orbital as a result. The potential barrier rises, the molecular orbitals de-hybridized into atomic orbitals, and the electrons are liberated on the atomic excited orbital when nuclei scatter in various cavities. Finally, two electrons emit a photon with modes Ω^\uparrow or Ω^\downarrow , and fall to the atomic ground orbital. The molecule disintegrates. Fig. 1(e) and Fig. 1(f) are three-dimensional surface diagrams that intuitively show how the potential wells around nuclei alter depending on how close or how far away they are.

In this paper we only consider two electrons with \downarrow as the initial condition. We suppose that every type of photon has a sufficiently large wavelength to interact with an electron located in any cavity.

The excited states of the electron with the spins for the first nucleus are indicated by $|0_1^\uparrow\rangle_e$ and $|0_1^\downarrow\rangle_e$. Usually simply written as $|0_1\rangle_e$, which can denote both $|0_1^\uparrow\rangle_e$

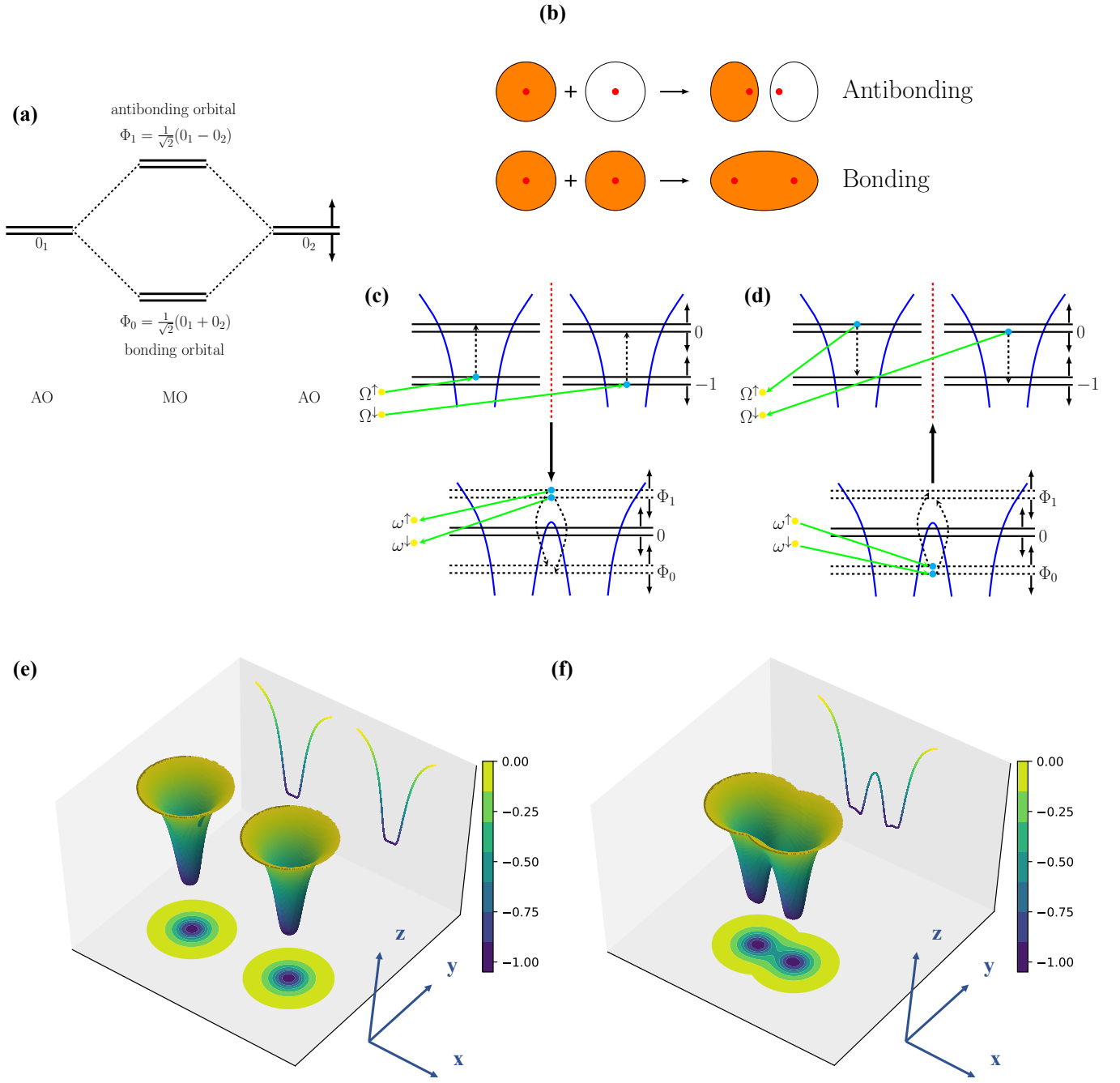


FIG. 1. (online color) *The association-dissociation model of neutral hydrogen molecule.* The hybridization of two hydrogen atoms' orbitals, as well as bonding and antibonding orbitals, are shown in (a) and (b). The formation of H_2 caused by the association reaction of two hydrogen atoms is depicted in (c). The decomposition of H_2 caused by the dissociation reaction of these hydrogen atoms is depicted in (d). Potential wells of the dissociative system are described by (e) when the distance between the nuclei is large (two nuclei are in different cavities). Potential wells of the associative system are described by (f) when the distance between the nuclei is small (two nuclei are in the same cavity). Protons are seen in (b) as red dots. In the figures (c) and (d), the blue and yellow dots, respectively, stand for electrons and photons.

and $|0_1^\downarrow\rangle_e$. The first nucleus's ground electron states are then determined by $|-\mathbf{1}_1\rangle_e$. For the second nucleus — $|0_2\rangle_e$ and $|-\mathbf{1}_2\rangle_e$. Only at great distances between nuclei are the ground states possible (see Figs. 1(c) and 1(d), where a vertical red dashed line indicates a significant distance between the nuclei).

Possible only for atomic excited states $|0_{1,2}\rangle_e$ is orbital hybridization — the introduction of molecular states $|\Phi_0\rangle_e$ and $|\Phi_1\rangle_e$ corresponding to bonding and antibonding orbitals, respectively. Hybridization is impossible for the atomic ground states $|-\mathbf{1}_{1,2}\rangle_e$. Hybrid molecular states of the electron energy are denoted by

$$|\Phi_1\rangle_e = \frac{1}{\sqrt{2}}(|0_1\rangle_e - |0_2\rangle_e) \quad (1a)$$

$$|\Phi_0\rangle_e = \frac{1}{\sqrt{2}}(|0_1\rangle_e + |0_2\rangle_e) \quad (1b)$$

where $|\Phi_1\rangle_e$ is molecular excited state, $|\Phi_0\rangle_e$ is molecular ground state.

We introduce the second quantization, also known as the occupation number representation [38, 39], to prevent the difficulty that antisymmetrization causes from

becoming more complicated. In this approach, the quantum many-body states are represented in the Fock state basis, which are constructed by filling up each single-particle state with a certain number of identical particles

$$|Fock\rangle = |n_1, n_2, n_3, \dots, n_\alpha, \dots\rangle \quad (2)$$

In the single-particle state $|\alpha\rangle$, it signifies that there are n_α particles. The total number of particles N is equal to the sum of the occupation numbers, or $\sum_\alpha n_\alpha = N$. Due to the Pauli exclusion principle, the occupancy number n_α for fermions can only be 0 or 1 but it can be any non-negative integer for bosons. The many-body Hilbert space, also known as Fock space, is completely based on all of the Fock states. A linear collection of Fock states can be used to express any generic quantum many-body state. The creation and annihilation operators are introduced in the second quantization formalism to construct and handle the Fock states, giving researchers studying the quantum many-body theory useful tools.

As a result, the entire system's Hilbert space for quantum states is \mathcal{C} and takes the following form

$$|\Psi\rangle_C = |p_1\rangle_{\omega^\uparrow}|p_2\rangle_{\omega^\downarrow}|p_3\rangle_{\Omega^\uparrow}|p_4\rangle_{\Omega^\downarrow}|p_5\rangle_{\Omega^s}|l_1\rangle_{at_1}^{\uparrow}|l_2\rangle_{at_1}^{\downarrow}|l_3\rangle_{at_1}^{\uparrow}|l_4\rangle_{at_1}^{\downarrow}|l_5\rangle_{at_2}^{\uparrow}|l_6\rangle_{at_2}^{\downarrow}|l_7\rangle_{at_2}^{\uparrow}|l_8\rangle_{at_2}^{\downarrow}|k\rangle_n \quad (3)$$

where the numbers of molecule photons with the modes $\omega^\uparrow, \omega^\downarrow$ are p_1, p_2 , respectively; p_3, p_4 are the numbers of atomic photons with modes $\Omega^\uparrow, \Omega^\downarrow$, respectively; p_5 is the number of photons with mode Ω^s , which can excite the electron spin from \downarrow to \uparrow in the atom. $l_{i,i \in \{1,2,\dots,8\}}$ describes orbital state (each atom has four orbitals: $0^\uparrow, 0^\downarrow, -1^\uparrow$ and -1^\downarrow): $l_i = 1$ — the orbital is occupied by one electron, $l_i = 0$ — the orbital is freed. The states of the nuclei are denoted by $|k\rangle_n$: $k = 0$ — state of nuclei, gathering together in one cavity, $k = 1$ — state of nuclei,

scattering in different cavities.

The space of quantum states \mathcal{C} can be absolutely separated to two subspaces \mathcal{A} and \mathcal{D} , where $\mathcal{A} \oplus \mathcal{D} = \mathcal{C}$, $\mathcal{A} \cap \mathcal{D} = \vec{0}$. The subspace for associative system, also known as molecular system, in which states correspond to $|0\rangle_n$, is \mathcal{A} . The subspace for dissociative system, also known as atomic system, in which the states correspond to $|1\rangle_n$, is \mathcal{D} . The following are the definitions for \mathcal{A} and \mathcal{D}

$$\mathcal{A} = c_0 \sum_{\substack{p_{i_1, i_1} \in \{1,2,\dots,5\}, \\ l_{i_2, i_2} \in \{1,2,\dots,8\}}} |p_1\rangle_{\omega^\uparrow}|p_2\rangle_{\omega^\downarrow}|p_3\rangle_{\Omega^\uparrow}|p_4\rangle_{\Omega^\downarrow}|p_5\rangle_{\Omega^s}|l_1\rangle_{at_1}^{\uparrow}|l_2\rangle_{at_1}^{\downarrow}|l_3\rangle_{at_1}^{\uparrow}|l_4\rangle_{at_1}^{\downarrow}|l_5\rangle_{at_2}^{\uparrow}|l_6\rangle_{at_2}^{\downarrow}|l_7\rangle_{at_2}^{\uparrow}|l_8\rangle_{at_2}^{\downarrow}|0\rangle_n \quad (4a)$$

$$\mathcal{D} = c_1 \sum_{\substack{p_{i_1, i_1} \in \{1,2,\dots,5\}, \\ l_{i_2, i_2} \in \{1,2,\dots,8\}}} |p_1\rangle_{\omega^\uparrow}|p_2\rangle_{\omega^\downarrow}|p_3\rangle_{\Omega^\uparrow}|p_4\rangle_{\Omega^\downarrow}|p_5\rangle_{\Omega^s}|l_1\rangle_{at_1}^{\uparrow}|l_2\rangle_{at_1}^{\downarrow}|l_3\rangle_{at_1}^{\uparrow}|l_4\rangle_{at_1}^{\downarrow}|l_5\rangle_{at_2}^{\uparrow}|l_6\rangle_{at_2}^{\downarrow}|l_7\rangle_{at_2}^{\uparrow}|l_8\rangle_{at_2}^{\downarrow}|1\rangle_n \quad (4b)$$

where c_0, c_1 are normalization factors.

The association-dissociation model of the neutral hydrogen molecule used in this paper is an adaptation of the TCHM that incorporates a multi-mode electromagnetic field inside optical cavities. The standard TCM

describes the interaction of N two-level atoms with a single-mode electromagnetic field inside an optical cavity and has been generalized to several cavities coupled by an optical fibre - the standard TCHM. First, the dynamics of system is described by solving the QME for the den-

sity matrix with the Lindblad operators of photon leakage from the cavity to external environment. The QME in the Markovian approximation for the density operator ρ of the system takes the following form

$$\begin{aligned} i\hbar\dot{\rho} &= \mathcal{L}(\rho) \\ &= [H, \rho] + iL(\rho) \end{aligned} \quad (5)$$

where \mathcal{L} is Lindblad superoperator and $[H, \rho] = H\rho - \rho H$ is the commutator. We have a graph \mathcal{K} of the potential photon dissipations between the states that are permitted. The edges and vertices of \mathcal{K} represent the permitted dissipations and the states, respectively. Similar to this, \mathcal{K}' is a graph of potential photon influxes that are permitted. $L(\rho)$ is as follows

$$L(\rho) = \sum_{k \in \mathcal{K}} L_k(\rho) + \sum_{k' \in \mathcal{K}'} L_{k'}(\rho) \quad (6)$$

where $L_k(\rho)$ is the standard dissipation superoperator corresponding to the jump operator A_k and taking as an argument on the density matrix ρ

$$L_k(\rho) = \gamma_k \left(A_k \rho A_k^\dagger - \frac{1}{2} \{ \rho, A_k^\dagger A_k \} \right) \quad (7)$$

where $\{ \rho, A_k^\dagger A_k \} = \rho A_k^\dagger A_k + A_k^\dagger A_k \rho$ is the anticommutator. The term γ_k refers to the overall spontaneous emission rate for photons for $k \in \mathcal{K}$ caused by photon leakage from the cavity to the external environment. Similarly, $L_{k'}(\rho)$ is the standard influx superoperator, having the following form

$$L_{k'}(\rho) = \gamma_{k'} \left(A_{k'}^\dagger \rho A_{k'} - \frac{1}{2} \{ \rho, A_{k'} A_{k'}^\dagger \} \right) \quad (8)$$

The total spontaneous influx rate for photon for $k' \in \mathcal{K}'$ is denoted by $\gamma_{k'}$.

The coupled-system Hamiltonian of the association-dissociation model in Eq. (5) is expressed by the total energy operator

$$H = H_{\mathcal{A}} + H_{\mathcal{D}} + H_{tun} \quad (9)$$

where H_{tun} denotes the quantum tunnelling effect between $H_{\mathcal{A}}$ and $H_{\mathcal{D}}$, which are the associative and dissociative Hamiltonians, respectively, that correspond to \mathcal{A} and \mathcal{D} .

$H_{\mathcal{A}}$ has following form

$$H_{\mathcal{A}} = \sigma_n \sigma_n^\dagger (H_{\mathcal{A},field} + H_{\mathcal{A},mol} + H_{\mathcal{A},int}) \quad (10)$$

where $\sigma_n \sigma_n^\dagger$ verifies that nuclei are close.

Rotating wave approximation (RWA) is taken into account. This approach ignores the quickly oscillating terms $\sigma^\dagger a^\dagger$, σa in a Hamiltonian. When the strength of the applied electromagnetic radiation is close to resonance with an atomic transition and the intensity is low, this approximation holds true [40]. Thus,

$$\frac{g}{\hbar\omega_c} \approx \frac{g}{\hbar\omega_n} \ll 1 \quad (11)$$

where ω_c stands for cavity frequency; and ω_n for transition frequency, which includes ω (ω^\uparrow and ω^\downarrow) for molecule, and Ω (Ω^\uparrow and Ω^\downarrow) for atom. RWA allows us to change $(\sigma^\dagger + \sigma)(a^\dagger + a)$ to $\sigma^\dagger a + \sigma a^\dagger$ in Eqs. (12c) and (14c). We typically presume that $\omega_c = \omega_n$. Thus,

$$H_{\mathcal{A},field} = \hbar\omega^\uparrow a_{\omega^\uparrow}^\dagger a_{\omega^\uparrow} + \hbar\omega^\downarrow a_{\omega^\downarrow}^\dagger a_{\omega^\downarrow} \quad (12a)$$

$$H_{\mathcal{A},mol} = \hbar\omega^\uparrow \sigma_{\omega^\uparrow}^\dagger \sigma_{\omega^\uparrow} + \hbar\omega^\downarrow \sigma_{\omega^\downarrow}^\dagger \sigma_{\omega^\downarrow} \quad (12b)$$

$$\begin{aligned} H_{\mathcal{A},int}^{RWA} &= g_{\omega^\uparrow} \left(\sigma_{\omega^\uparrow}^\dagger a_{\omega^\uparrow} + \sigma_{\omega^\uparrow} a_{\omega^\uparrow}^\dagger \right) \\ &+ g_{\omega^\downarrow} \left(\sigma_{\omega^\downarrow}^\dagger a_{\omega^\downarrow} + \sigma_{\omega^\downarrow} a_{\omega^\downarrow}^\dagger \right) \end{aligned} \quad (12c)$$

where $\hbar = h/2\pi$ is the reduced Planck constant or Dirac constant. $H_{\mathcal{A},field}$ is the photon energy operator, $H_{\mathcal{A},mol}$ is the molecule energy operator, $H_{\mathcal{A},int}$ is the molecule-photon interaction operator. g_ω is the coupling strength between the photon mode ω (with annihilation and creation operators a_ω and a_ω^\dagger , respectively) and the electrons in the molecule (with excitation and relaxation operators σ_ω^\dagger and σ_ω , respectively).

Then $H_{\mathcal{D}}$ is described in following form

$$H_{\mathcal{D}} = \sigma_n^\dagger \sigma_n (H_{\mathcal{D},field} + H_{\mathcal{D},mol} + H_{\mathcal{D},int}) \quad (13)$$

where $\sigma_n^\dagger \sigma_n$ verifies that nuclei are far away. Similarly, we introduce RWA

$$H_{\mathcal{D},field} = \hbar\Omega^\uparrow a_{\Omega^\uparrow}^\dagger a_{\Omega^\uparrow} + \hbar\Omega^\downarrow a_{\Omega^\downarrow}^\dagger a_{\Omega^\downarrow} \quad (14a)$$

$$H_{\mathcal{D},at} = \sum_{i=1,2} \left(\hbar\Omega^\uparrow \sigma_{\Omega^\uparrow,i}^\dagger \sigma_{\Omega^\uparrow,i} + \hbar\Omega^\downarrow \sigma_{\Omega^\downarrow,i}^\dagger \sigma_{\Omega^\downarrow,i} \right) \quad (14b)$$

$$\begin{aligned} H_{\mathcal{D},int}^{RWA} &= \sum_{i=1,2} \left\{ g_{\Omega^\uparrow} \left(\sigma_{\Omega^\uparrow,i}^\dagger a_{\Omega^\uparrow} + \sigma_{\Omega^\uparrow,i} a_{\Omega^\uparrow}^\dagger \right) \right. \\ &\quad \left. + g_{\Omega^\downarrow} \left(\sigma_{\Omega^\downarrow,i}^\dagger a_{\Omega^\downarrow} + \sigma_{\Omega^\downarrow,i} a_{\Omega^\downarrow}^\dagger \right) \right\} \end{aligned} \quad (14c)$$

where $H_{\mathcal{D},field}$ is the photon energy operator, $H_{\mathcal{D},at}$ is the atom energy operator, $H_{\mathcal{D},int}$ is atom-photon interaction operator. g_Ω is the coupling strength between the photon mode Ω (with annihilation and creation operators a_Ω and a_Ω^\dagger , respectively) and the electrons in the atom (with excitation and relaxation operators $\sigma_{\Omega,i}^\dagger$ and $\sigma_{\Omega,i}$, respectively, here i denotes index of atoms).

Finally, H_{tun} describe the hybridization and dehybridization, realized by quantum tunnelling effect, it takes the form

$$\begin{aligned} H_{tun} &= \zeta_2 \sigma_{\omega^\uparrow}^\dagger \sigma_{\omega^\uparrow} \sigma_{\omega^\downarrow}^\dagger \sigma_{\omega^\downarrow} (\sigma_n^\dagger + \sigma_n) \\ &+ \zeta_1 \sigma_{\omega^\uparrow} \sigma_{\omega^\uparrow}^\dagger \sigma_{\omega^\downarrow}^\dagger \sigma_{\omega^\downarrow} (\sigma_n^\dagger + \sigma_n) \\ &+ \zeta_1 \sigma_{\omega^\uparrow}^\dagger \sigma_{\omega^\uparrow} \sigma_{\omega^\downarrow} \sigma_{\omega^\downarrow}^\dagger (\sigma_n^\dagger + \sigma_n) \\ &+ \zeta_0 \sigma_{\omega^\uparrow} \sigma_{\omega^\uparrow}^\dagger \sigma_{\omega^\downarrow} \sigma_{\omega^\downarrow}^\dagger (\sigma_n^\dagger + \sigma_n) \end{aligned} \quad (15)$$

where $\sigma_{\omega^\uparrow}^\dagger \sigma_{\omega^\uparrow} \sigma_{\omega^\downarrow}^\dagger \sigma_{\omega^\downarrow}$ verifies that two electrons with different spins are at orbital Φ_1 with large tunnelling intensity ζ_2 ; $\sigma_{\omega^\uparrow} \sigma_{\omega^\uparrow}^\dagger \sigma_{\omega^\downarrow}^\dagger \sigma_{\omega^\downarrow}$ verifies that electron with \uparrow is at orbital Φ_0 and electron with \downarrow is at orbital Φ_1 , with low

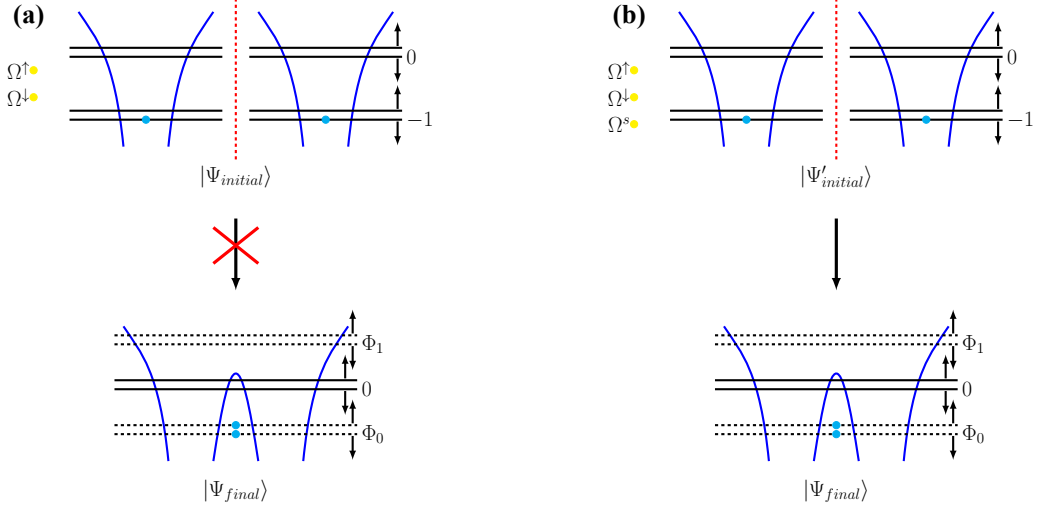


FIG. 2. (online color) *Electron spin transition*. The situation without consideration of electron spin transition is depicted in (a), where it is impossible to construct a neutral hydrogen molecule if only two photons with the same modes Ω^\downarrow are present at the beginning. The situation, which takes into account the electron spin transition, is depicted in (b), where the addition of a photon with the mode Ω^s can result in the formation of a neutral hydrogen molecule.

tunnelling intensity ζ_1 ; $\sigma_{\omega\uparrow}^\dagger \sigma_{\omega\uparrow} \sigma_{\omega\downarrow} \sigma_{\omega\downarrow}^\dagger$ verifies that electron with \uparrow is at orbital Φ_1 and electron with \downarrow is at orbital Φ_0 , with low tunnelling intensity ζ_1 ; $\sigma_{\omega\uparrow} \sigma_{\omega\uparrow}^\dagger \sigma_{\omega\downarrow} \sigma_{\omega\downarrow}^\dagger$ verifies that two electrons with different spins are at orbital Φ_0 with tunnelling intensity ζ_0 , which equal to 0. In a nutshell, the quantum tunnelling effect is diminished when an electron fall to the molecular ground state.

On a p-photon state, the photon annihilation and creation operators are described as

$$\begin{aligned} \text{if } p > 0, & \begin{cases} a_\omega |p\rangle_\omega = \sqrt{p}|p-1\rangle_\omega, \\ a_\omega^\dagger |p\rangle_\omega = \sqrt{p+1}|p+1\rangle_\omega, \\ a_\Omega |p\rangle_\Omega = \sqrt{p}|p-1\rangle_\Omega, \\ a_\Omega^\dagger |p\rangle_\Omega = \sqrt{p+1}|p+1\rangle_\Omega, \end{cases} \\ \text{if } p = 0, & \begin{cases} a_\omega |0\rangle_\omega = 0, \\ a_\omega^\dagger |0\rangle_\omega = |1\rangle_\omega, \\ a_\Omega |0\rangle_\Omega = 0, \\ a_\Omega^\dagger |0\rangle_\Omega = |1\rangle_\Omega. \end{cases} \end{aligned} \quad (16)$$

The interaction of molecule with the electromagnetic field of the cavity, emitting or absorbing photon with mode $\omega^{\uparrow,\downarrow}$, is described as

$$\begin{aligned} \sigma_\omega |1\rangle_{\Phi_1} |0\rangle_{\Phi_0} &= |0\rangle_{\Phi_1} |1\rangle_{\Phi_0}, \\ \sigma_\omega^\dagger |0\rangle_{\Phi_1} |1\rangle_{\Phi_0} &= |1\rangle_{\Phi_1} |0\rangle_{\Phi_0}. \end{aligned} \quad (17)$$

The interaction of atom with the electromagnetic field of the cavity, emitting or absorbing photon with mode $\Omega^{\uparrow,\downarrow}$, is described as

$$\begin{aligned} \sigma_{\Omega,i} |1\rangle_{or_0} |0\rangle_{or_{-1}} &= |0\rangle_{or_0} |1\rangle_{or_{-1}}, \\ \sigma_{\Omega,i}^\dagger |0\rangle_{or_0} |1\rangle_{or_{-1}} &= |1\rangle_{or_0} |0\rangle_{or_{-1}}. \end{aligned} \quad (18)$$

The nuclei's tunnelling operators, $\sigma_n, \sigma_n^\dagger$, have following form

$$\begin{aligned} \sigma_n |1\rangle_n &= |0\rangle_n, \\ \sigma_n^\dagger |0\rangle_n &= |1\rangle_n. \end{aligned} \quad (19)$$

III. ELECTRON SPIN TRANSITION

The association-dissociation model is introduced with spin photons with mode Ω^s in this section, allowing for transitions between \uparrow and \downarrow . The Pauli exclusion principle, which prohibits the presence of electrons with the same spin at the same energy level, must be carefully followed by electron spins. We agree that an electron spin transition is only possible if the electrons are in the atomic states corresponding to $|1\rangle_n$. Electron spin transition is forbidden when electrons are in molecular states corresponding to $|0\rangle_n$, which contravenes Pauli exclusion principle. Only a state with two electrons in orbital Φ_0 with different spins can result in the stable formation of H_2 . This situation is just right accord with that a stable system has a lower energy level, this position is ideal.

Similarly to Eq. (16), the photon annihilation and creation operators on an p-photon state with mode Ω^s are described as

$$\begin{aligned} \text{if } p > 0, & \begin{cases} a_{\Omega^s} |p\rangle_{\Omega^s} = \sqrt{p}|p-1\rangle_{\Omega^s}, \\ a_{\Omega^s}^\dagger |p\rangle_{\Omega^s} = \sqrt{p+1}|p+1\rangle_{\Omega^s}, \end{cases} \\ \text{if } p = 0, & \begin{cases} a_{\Omega^s} |0\rangle_{\Omega^s} = 0, \\ a_{\Omega^s}^\dagger |0\rangle_{\Omega^s} = |1\rangle_{\Omega^s}. \end{cases} \end{aligned} \quad (20)$$

And the interaction of atom with the electromagnetic field of the cavity, emitting or absorbing photon with

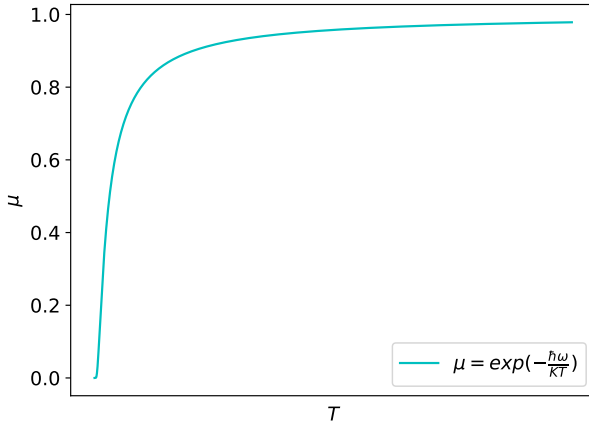


FIG. 3. (online color) *Temperature variations.* The curve of the temperature-dependent function μ is depicted by the cyan solid curve.

mode Ω^s and causing spin-flip, is described as

$$\begin{aligned} \sigma_{\Omega^s,i} |1\rangle_{\substack{at_i \\ or_0}}^{\uparrow} |0\rangle_{\substack{at_i \\ or_0}}^{\downarrow} &= |0\rangle_{\substack{at_i \\ or_0}}^{\uparrow} |1\rangle_{\substack{at_i \\ or_0}}^{\downarrow}, \\ \sigma_{\Omega^s,i} |1\rangle_{\substack{at_i \\ or_{-1}}}^{\uparrow} |0\rangle_{\substack{at_i \\ or_{-1}}}^{\downarrow} &= |0\rangle_{\substack{at_i \\ or_{-1}}}^{\uparrow} |1\rangle_{\substack{at_i \\ or_{-1}}}^{\downarrow}, \\ \sigma_{\Omega^s,i}^{\dagger} |0\rangle_{\substack{at_i \\ or_0}}^{\uparrow} |1\rangle_{\substack{at_i \\ or_0}}^{\downarrow} &= |1\rangle_{\substack{at_i \\ or_0}}^{\uparrow} |0\rangle_{\substack{at_i \\ or_0}}^{\downarrow}, \\ \sigma_{\Omega^s,i}^{\dagger} |0\rangle_{\substack{at_i \\ or_{-1}}}^{\uparrow} |1\rangle_{\substack{at_i \\ or_{-1}}}^{\downarrow} &= |1\rangle_{\substack{at_i \\ or_{-1}}}^{\uparrow} |0\rangle_{\substack{at_i \\ or_{-1}}}^{\downarrow}. \end{aligned} \quad (21)$$

where i denotes index of atoms.

We consider two situations:

- in Fig. 2(a) we only pump into two photons with different modes Ω^{\uparrow} and Ω^{\downarrow} , and spin photons are proviso not taken into consideration, and transition between \uparrow and \downarrow is prohibited;
- in Fig. 2(b) spin photons and corresponding transition is introduced.

Theoretically, the formation of H_2 is thus impossible in the first situation, and is achieved in the second situation.

IV. THERMALLY STATIONARY STATE

As a mixed state with a Gibbs distribution of Fock components, we define the stationary state of a field with temperature T as follows

$$\mathcal{G}(T)_f = c \sum_{p=0}^{\infty} \exp\left(-\frac{\hbar\omega_c p}{KT}\right) |p\rangle \langle p|, \quad (22)$$

where K is the Boltzmann constant, c is the normalization factor, p is the number of photons, ω_c is the photonic

mode. The notation $\gamma_{k'}/\gamma_k = \mu$ is presented. Since the temperature would otherwise be endlessly high and the state $\mathcal{G}(T)_f$ would not be normalizable, the state will then only exist at $\mu < 1$.

The probability of the photonic Fock state $|p\rangle$ at temperature T is proportional to $\exp(-\frac{\hbar\omega_c}{KT})$. In our model, we assume

$$\mu = \exp\left(-\frac{\hbar\omega_c}{KT}\right) \quad (23)$$

from where $T = \frac{\hbar\omega_c}{K \ln(1/\mu)}$.

The following theorem takes place as follows [41] and the proof of it is given in the Appx. B:

The thermally stationary state of atoms and fields at temperature T has the form $\rho_{state} = \rho_{ph} \otimes \rho_{at}$, where ρ_{ph} is the state of the photon and ρ_{at} is the state of the atom.

The curves of temperature-dependent function $\mu(T)$ is displayed in Fig. 3. When $T = 0$, $\mu = 0$, then μ rises sharply with the increase of temperature, and reaches plateau when T is large. If T is large enough, μ will be infinite close to 1.

V. THE MODEL WITH COVALENT BOND AND PHONON

Now, a simpler and more precise model featuring a covalent bond and a simple harmonic oscillator (phonon) is presented in Fig. 4. Both the association response and the dissociation reaction can be interpreted by this model. The dissociation reaction cannot be fully explained by the prior model.

The Hilbert space of quantum states of the entire system, having the following form

$$|\Psi\rangle_c = |p_1\rangle_{\omega^{\uparrow}} |p_2\rangle_{\omega^{\downarrow}} |m\rangle_{\Omega^c} |l_1\rangle_{\Phi_1^{\uparrow}} |l_2\rangle_{\Phi_1^{\downarrow}} |L\rangle_{cb} |k\rangle_n \quad (24)$$

where p_1, p_2 are the numbers of molecular photons with modes $\omega^{\uparrow}, \omega^{\downarrow}$, respectively; m is the number of phonons with mode Ω^c . l_1, l_2 describe orbital state: $l_1 = 1$ — electron with spin \uparrow in excited orbital Φ_1^{\uparrow} , $l_1 = 0$ — electron with spin \uparrow in ground orbital Φ_0^{\uparrow} ; $l_2 = 1$ — electron with spin \downarrow in excited orbital Φ_1^{\downarrow} , $l_2 = 0$ — electron with spin \downarrow in ground orbital Φ_0^{\downarrow} . The states of the covalent bond are denoted by $|L\rangle_{cb}$: $L = 0$ — covalent bond formation, $L = 1$ — covalent bond breaking. The states of the nuclei are denoted by $|k\rangle_n$: $k = 0$ — state of nuclei, gathering together in one cavity, $k = 1$ — state of nuclei, scattering in different cavities.

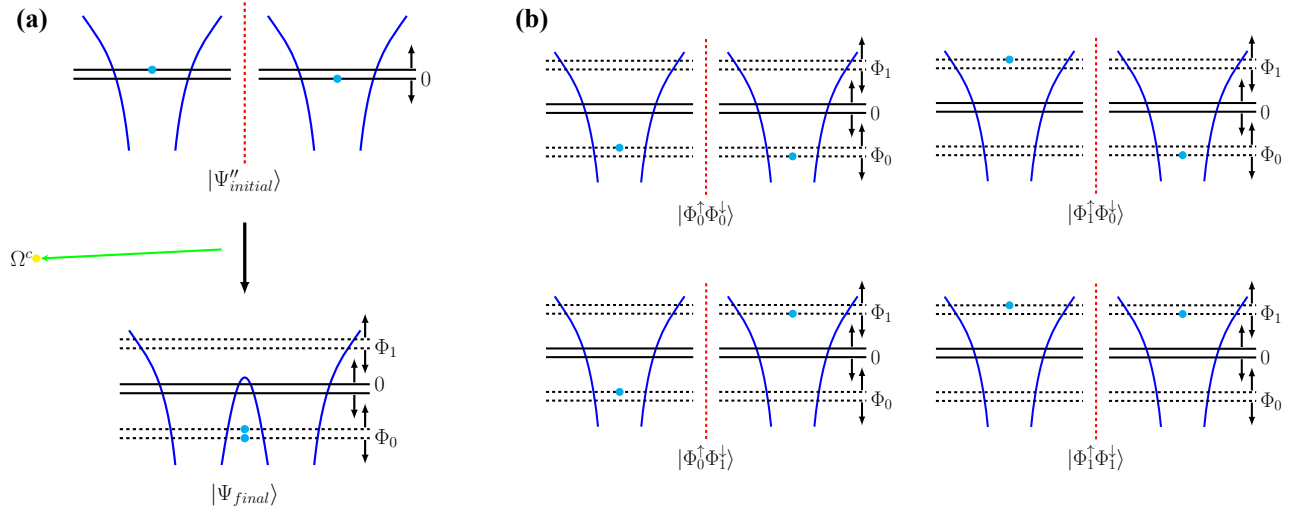


FIG. 4. (online color) *The model with covalent bond and phonon.* When nuclei are in distinct cavities in the model depicted in (a), electrons are constrained to orbital 0; however, when nuclei are in the same cavity, electrons can jump between orbitals Φ_1 and Φ_0 . In order to make a covalent bond, a phonon must be released, and in order to break a covalent link, a phonon must be absorbed. In (b), according to Eqs. (1), $|\Psi''_{initial}\rangle$ can be decomposed into the sum of four states $|\Phi_0^\uparrow\Phi_0^\downarrow\rangle$, $|\Phi_1^\uparrow\Phi_0^\downarrow\rangle$, $|\Phi_0^\uparrow\Phi_1^\downarrow\rangle$ and $|\Phi_1^\uparrow\Phi_1^\downarrow\rangle$.

Hamiltonian of this new model has following form

$$\begin{aligned}
 H_{cb}^{RW^A} = & \hbar\omega^{\uparrow}a_{\omega^{\uparrow}}^{\dagger}a_{\omega^{\uparrow}} + \hbar\omega^{\downarrow}a_{\omega^{\downarrow}}^{\dagger}a_{\omega^{\downarrow}} + \hbar\Omega^c a_{\Omega^c}^{\dagger}a_{\Omega^c} \\
 & + \hbar\omega^{\uparrow}\sigma_{\omega^{\uparrow}}^{\dagger}\sigma_{\omega^{\uparrow}} + \hbar\omega^{\downarrow}\sigma_{\omega^{\downarrow}}^{\dagger}\sigma_{\omega^{\downarrow}} + \hbar\Omega^c\sigma_{\Omega^c}^{\dagger}\sigma_{\Omega^c} \\
 & + g_{\omega^{\uparrow}}(a_{\omega^{\uparrow}}^{\dagger}\sigma_{\omega^{\uparrow}} + a_{\omega^{\uparrow}}\sigma_{\omega^{\uparrow}}^{\dagger}) \\
 & + g_{\omega^{\downarrow}}(a_{\omega^{\downarrow}}^{\dagger}\sigma_{\omega^{\downarrow}} + a_{\omega^{\downarrow}}\sigma_{\omega^{\downarrow}}^{\dagger}) \\
 & + g_{\Omega^c}(a_{\Omega^c}^{\dagger}\sigma_{\Omega^c} + a_{\Omega^c}\sigma_{\Omega^c}^{\dagger}) \\
 & + \zeta(\sigma_n^{\dagger}\sigma_n + \sigma_n\sigma_n^{\dagger})
 \end{aligned} \quad (25)$$

where g_{Ω^c} — strength of formation or breaking of covalent bond, ζ — tunnelling intensity.

Initial state $|\Psi''_{initial}\rangle$ is shown in Fig. 4 (a), which can be decomposed into the sum of four states

$$|\Psi''_{initial}\rangle = \frac{1}{2} \left(|\Phi_0^\uparrow\Phi_0^\downarrow\rangle + |\Phi_1^\uparrow\Phi_0^\downarrow\rangle - |\Phi_0^\uparrow\Phi_1^\downarrow\rangle - |\Phi_1^\uparrow\Phi_1^\downarrow\rangle \right) \quad (26)$$

where

$$|\Phi_0^\uparrow\Phi_0^\downarrow\rangle = |0\rangle_{\omega^{\uparrow}}|0\rangle_{\omega^{\downarrow}}|0\rangle_{\Omega^c}|0\rangle_{\Phi_1^{\uparrow}}|0\rangle_{\Phi_1^{\downarrow}}|1\rangle_{cb}|1\rangle_n \quad (27a)$$

$$|\Phi_1^\uparrow\Phi_0^\downarrow\rangle = |0\rangle_{\omega^{\uparrow}}|0\rangle_{\omega^{\downarrow}}|0\rangle_{\Omega^c}|1\rangle_{\Phi_1^{\uparrow}}|0\rangle_{\Phi_1^{\downarrow}}|1\rangle_{cb}|1\rangle_n \quad (27b)$$

$$|\Phi_0^\uparrow\Phi_1^\downarrow\rangle = |0\rangle_{\omega^{\uparrow}}|0\rangle_{\omega^{\downarrow}}|0\rangle_{\Omega^c}|0\rangle_{\Phi_1^{\uparrow}}|1\rangle_{\Phi_1^{\downarrow}}|1\rangle_{cb}|1\rangle_n \quad (27c)$$

$$|\Phi_1^\uparrow\Phi_1^\downarrow\rangle = |0\rangle_{\omega^{\uparrow}}|0\rangle_{\omega^{\downarrow}}|0\rangle_{\Omega^c}|1\rangle_{\Phi_1^{\uparrow}}|1\rangle_{\Phi_1^{\downarrow}}|1\rangle_{cb}|1\rangle_n \quad (27d)$$

It should be noted that $|\Phi_0^\uparrow\Phi_0^\downarrow\rangle$ shown in Fig. 4 (b) does not mean that there is the electron with \uparrow in the ground state of the atom on the left, and the electron with \downarrow in the ground state of the atom on the right. The exact reverse can be true. We only know that one of the atoms (we don't know which one) has the electron with \uparrow in the ground state, and that the other atom has the electron with \downarrow . This is because we employ second quantization. In Fig. 4 (b), for the convenience of explanation, we just intentionally fixed the electron with \uparrow on the left atom. The same is true for the other three states $|\Phi_1^\uparrow\Phi_0^\downarrow\rangle$, $|\Phi_0^\uparrow\Phi_1^\downarrow\rangle$ and $|\Phi_1^\uparrow\Phi_1^\downarrow\rangle$.

Now we define $\{0 \succ_{cb}$ and $\{1 \succ_{cb}$, which have following forms

$$\{0 \succ_{cb} = c_2 \sum_{p_1, p_2, m, l_1, l_2, k} |p_1\rangle_{\omega^\uparrow} |p_2\rangle_{\omega^\downarrow} |m\rangle_{\Omega^c} |l_1\rangle_{\Phi_1^\uparrow} |l_2\rangle_{\Phi_1^\downarrow} |0\rangle_{cb} |k\rangle_n \quad (28a)$$

$$\{1 \succ_{cb} = c_3 \sum_{p_1, p_2, m, l_1, l_2, k} |p_1\rangle_{\omega^\uparrow} |p_2\rangle_{\omega^\downarrow} |m\rangle_{\Omega^c} |l_1\rangle_{\Phi_1^\uparrow} |l_2\rangle_{\Phi_1^\downarrow} |1\rangle_{cb} |k\rangle_n \quad (28b)$$

where c_2, c_3 are normalization factors.

VI. NUMERICAL METHOD

The solution $\rho(t)$ in Eq. (5) may be approximately found as a sequence of two steps: in the first step we make one step in the solution of the unitary part of Eq. (5)

$$\tilde{\rho}(t+dt) = \exp(-\frac{i}{\hbar}Hdt)\rho(t)\exp(\frac{i}{\hbar}Hdt) \quad (29)$$

and in the second step, make one step in the solution of Eq. (5) with the commutator removed:

$$\rho(t+dt) = \tilde{\rho}(t+dt) + \frac{1}{\hbar}L(\tilde{\rho}(t+dt))dt \quad (30)$$

We have the conventional technique known as tensor product for establishing Hamiltonian in Eq. (29). Through the use of the tensor product, we can directly establish the Hamiltonian with Eq. (9); however, the dimension of the Hamiltonian that results from this method is frequently very large and contains a lot of excess states that are not involved in evolution, particularly when the degree of freedom of the system is high. In this section, we'll introduce the generator algorithm (comparison between tensor product and generator algorithm is shown in Appx. C), which is based on the occupation number representation in Eq. (3), and includes the following two steps:

- generating and numbering potential evolution states involved in the evolution in accordance with the initial state and any its potential dissipative states that may be relevant in solving QME;
- establishing Hamiltonian with these states and potential interactions and dissipations among them.

Using this technique, we now eliminate the extra unnecessary states and obtain anew \mathcal{C}' and H' , where $\mathcal{C}' \subset \mathcal{C}$ and $\dim(H') \leq \dim(H)$. In this paper, the $\dim(H') \approx 100$ is far smaller than the $\dim(H) = 2^{14} = 16384$. As a result, complexity is reduced. The effectiveness of this reduction strategy increases with the increase of degree of freedom for multi-particle systems.

VII. SIMULATIONS AND RESULTS

The coupling strength of photon and the electron in the cavity takes the form:

$$g_n = \sqrt{\hbar\omega_n b/V}dE(x) \quad (31)$$

where ω_n is transition frequency, V is the effective volume of the cavity, d is the dipole moment of the transition between the ground and the perturbed states and $E(x)$ describes the spatial arrangement of the atom in the cavity, which has the form $E(x) = \sin(\pi x/l)$, here l is the length of the cavity. To ensure the confinement of the photon in the cavity, l has to be chosen such that $l = r\lambda/2$ is a multiple of the photon wavelength λ . In experiments, $r = 1$ is often chosen to decrease the effective volume of the cavity, which makes it possible to obtain dozens of Rabi oscillations [42]. We assume that $\Omega^c < \Omega^s < \omega^\uparrow = \omega^\downarrow < \Omega^\uparrow = \Omega^\downarrow$, thus $g_{\Omega^c} < g_{\Omega^s} < g_{\omega^\uparrow} = g_{\omega^\downarrow} < g_{\Omega^\uparrow} = g_{\Omega^\downarrow}$ according to Eq. (31).

In simulations:

$$\Omega^\uparrow = \Omega^\downarrow, \omega^\uparrow = \omega^\downarrow = 0.5 * \Omega^\uparrow, \Omega^s = 0.1 * \Omega^\uparrow, \Omega^c = 0.01 * \Omega^\uparrow;$$

$$g_{\Omega^\uparrow} = g_{\Omega^\downarrow} = 0.01 * \Omega^\uparrow, g_{\omega^\uparrow} = g_{\omega^\downarrow} = 0.5 * g_{\Omega^\uparrow}, g_{\Omega^s} = 0.1 * g_{\Omega^\uparrow}, g_{\Omega^c} = 0.05 * g_{\Omega^\uparrow};$$

$$\zeta = 0.5 * g_{\Omega^\uparrow}, \zeta_2 = 10 * g_{\Omega^\uparrow}, \zeta_1 = g_{\Omega^\uparrow}, \zeta_0 = 0.$$

In Markovian open systems, we assume that the dissipative rates of all types of photon leakage are equal:

$$\gamma_{\omega^\uparrow} = \gamma_{\omega^\downarrow} = \gamma_{\Omega^\uparrow} = \gamma_{\Omega^\downarrow} = \gamma_{\Omega^s} = \gamma_{\Omega^c} = 0.1 * g_{\Omega^\uparrow}.$$

A. Without consideration of electron spin transition

In this subsection, a photon with mode Ω^\uparrow and a photon with mode Ω^\downarrow are the only ones pumped into the system at the beginning, corresponding to the initial state $|\Psi_{initial}\rangle$, described in Fig. 2 (a), where two electrons with \downarrow are in atomic ground state of different atoms, and photon with mode Ω^s , which can excite electron from \downarrow to \uparrow , is absent. Electron spin transition is thus prohibited. Additionally, only the influx of photons with modes Ω^\uparrow and Ω^\downarrow is taken into account. The influx of photons with modes ω^\uparrow and ω^\downarrow is forbidden. And as stated in Sec. IV, the influx rate is always lower than the corresponding dissipative rate.

We assume that $\mu_{\omega^\uparrow} = \mu_{\omega^\downarrow} = 0$, $\mu_{\Omega^\uparrow} = \mu_{\Omega^\downarrow} = 0.5$.

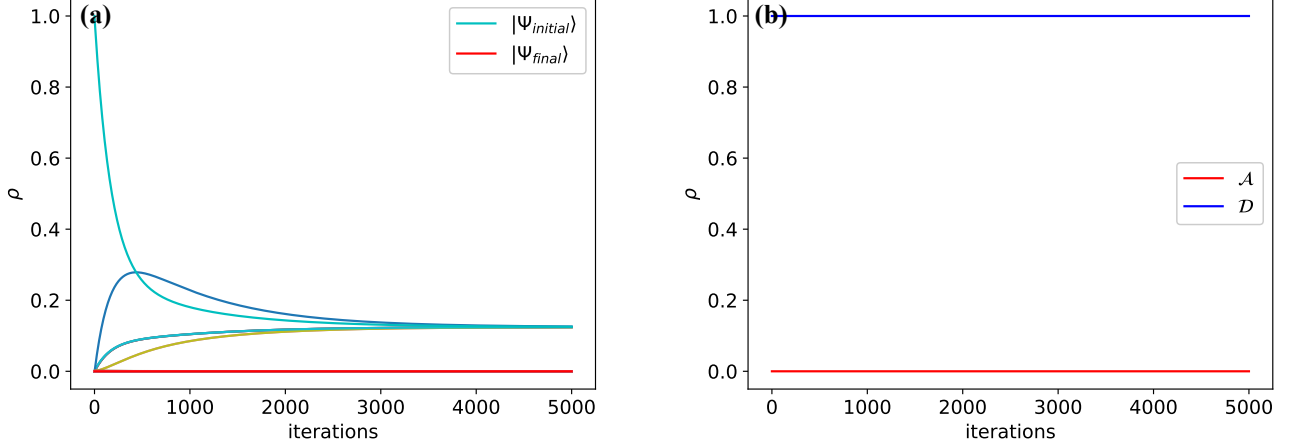


FIG. 5. (online color) *The evolution without consideration of electron spin transition.* (a) shows the curves of time-dependent probabilities of all possible states involved in the evolution. Probability of state $|\Psi_{initial}\rangle$ is denoted by cyan solid curve, and probability of state $|\Psi_{final}\rangle$ is denoted by red solid curve. (b) shows the curves of time-dependent probabilities of subspaces \mathcal{A} and \mathcal{D} . Probability of \mathcal{A} is denoted by red solid curve, and probability of \mathcal{D} is denoted by blue solid curve.

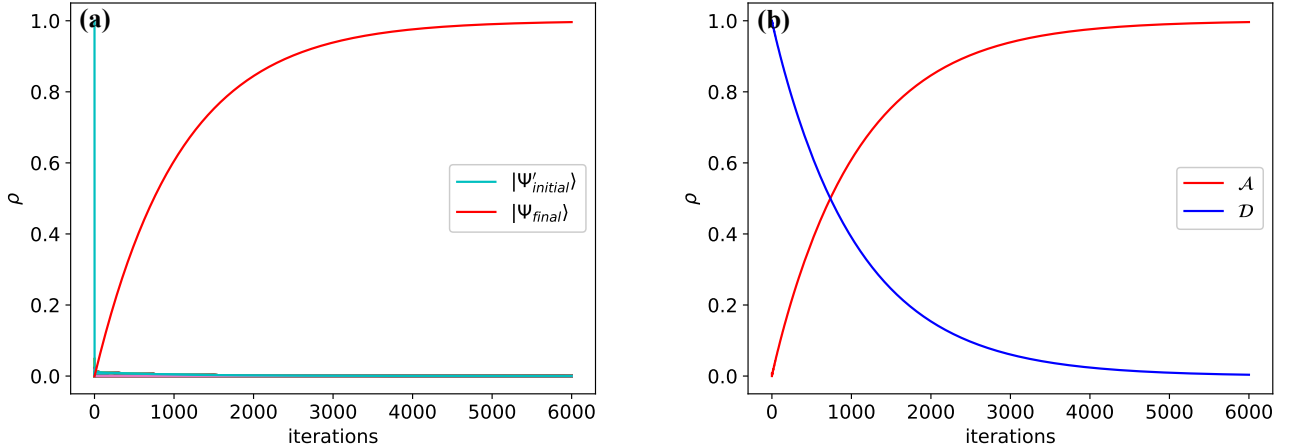


FIG. 6. (online color) *The evolution with consideration of electron spin transition.* In (a), probability of state $|\Psi'_{initial}\rangle$ is denoted by cyan solid curve. Other curves represent as same in Fig. 5.

In Fig. 2 two electrons with different spins are anchored in the molecular ground orbital, describing the $|\Psi_{final}\rangle$. Theoretically, it is impossible to accomplish $|\Psi_{final}\rangle$ because hybridization of atomic orbitals only occurs when two electrons in identically excited atomic orbitals have different spins. The red solid curve representing $|\Psi_{final}\rangle$ is always equal to 0 during the whole evolution, as shown by the numerical results in Fig. 5(a). And in Fig. 5(b), red solid curve representing \mathcal{A} , which is the sum of probabilities of all states belonging to associative system corresponding to $|0\rangle_n$, is also always equal to 0. And blue solid curve representing \mathcal{D} , which is the

sum of probabilities of all states belonging to dissociative system corresponding to $|1\rangle_n$, is always equal to 1. This indicates that no energy enters the associative system throughout evolution in our model, and the entire system remains completely dissociated. This means that when two electrons are both fixed with the same spin, and when electron spin transition is inhibitive, formation of the neutral hydrogen molecule is impossible.

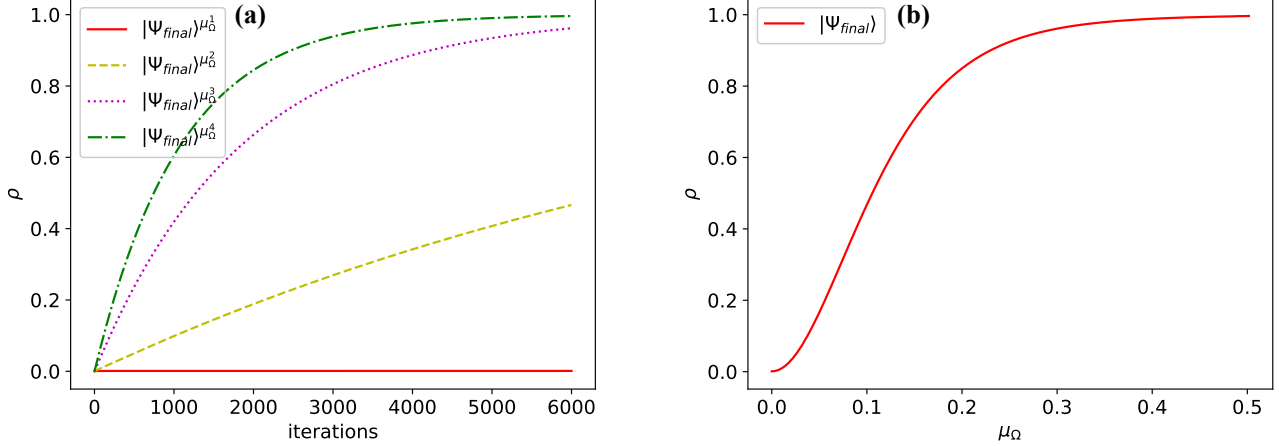


FIG. 7. (online color) Temperature variation of photonic modes Ω^\uparrow and Ω^\downarrow . In (a), time-dependent curves of $|\Psi_{final}\rangle$ are corresponding to μ_{Ω^1} (red solid), μ_{Ω^2} (yellow dashed), μ_{Ω^3} (magenta dotted) and μ_{Ω^4} (green dash-dotted), respectively. In (b), red curve represents the probability of $|\Psi_{final}\rangle$ when iterations reaches 6000, with the increase of μ_Ω from 0 to 0.5.

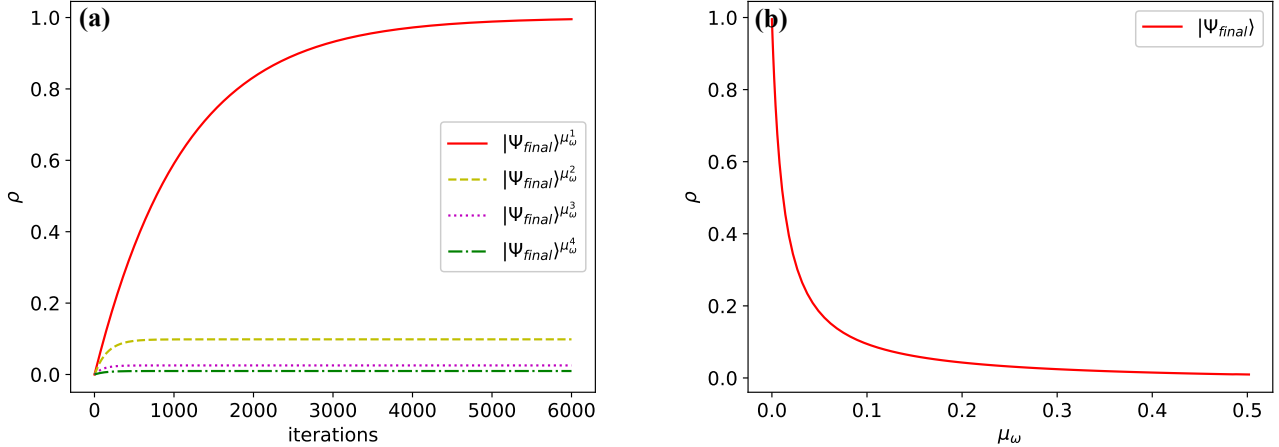


FIG. 8. (online color) Temperature variation of photonic modes ω^\uparrow and ω^\downarrow . In (a), time-dependent curves of $|\Psi_{final}\rangle$ are corresponding to μ_{ω^1} (red solid), μ_{ω^2} (yellow dashed), μ_{ω^3} (magenta dotted) and μ_{ω^4} (green dash-dotted), respectively. In (b), red curve represents the probability of $|\Psi_{final}\rangle$ when iterations reaches 6000, with the increase of μ_ω from 0 to 0.5.

B. With consideration of electron spin transition

The association-dissociation model of the neutral hydrogen molecule now includes the spin-flip photon, and electron spin transition is a possibility. According to Fig. 2 (b), the initial state is $|\Psi'_{initial}\rangle$, where a photon with the mode Ω^s is introduced. We further stipulate that an electron can only undergo an electron spin transition when it is in an atomic state, both excited and ground.

Similarly, for added photon with mode Ω^s , we assume that $\mu_{\Omega^s} = 0.5$. Others as same in Subsec. VII A.

According to numerical results in Fig. 6(a), we discov-

ered that the red solid curve $|\Psi_{final}\rangle$ climbs and reaches 1 at the end when electron spin transition is taken into account. It indicates that the formation of H_2 has been accomplished and that there are no longer any free hydrogen atoms. Additionally, the red solid curve \mathcal{A} rises and reaches 1 in Fig. 6(b), while the blue solid curve \mathcal{D} declines to 0. In other words, when electron spin transition is allowed, the formation of a neutral hydrogen molecule is conceivable when two electrons have different spins.

We make the assumption that the dissipative rate of all types of photons is the same, which is why what is depicted in Fig. 6 is accurate. μ_{Ω^\uparrow} , μ_{Ω^\downarrow} and μ_{Ω^s} are

equal to 0.5, and $\mu_{\omega\uparrow}$, $\mu_{\omega\downarrow} = 0$ (which means that the inflow rates of photons with the modes ω^\uparrow and ω^\downarrow are both 0). In order to force electrons to move from the molecular ground orbital to the excited orbital, as shown in Fig. 1(d), the decomposition of hydrogen molecules must absorb photons with modes ω^\uparrow and ω^\downarrow , but because these photons cannot be replenished, they will gradually leak until they are completely absent in the cavity. As a result, the system finally evolves over time to generate a stable neutral hydrogen molecule.

C. Temperature variation

We are currently looking at how changes in temperature affect the evolution and the formation of neutral hydrogen molecules using the photonic modes Ω^\uparrow , Ω^\downarrow , ω^\uparrow , ω^\downarrow and Ω^s . Fig. 3 displays the temperature-dependent function μ , which increases along with the temperature.

In this subsection we use μ instead of temperature T as the abscissa, and for convenience suppose $\mu_\Omega = \mu_{\Omega^\uparrow} = \mu_{\Omega^\downarrow}$ and $\mu_\omega = \mu_{\omega^\uparrow} = \mu_{\omega^\downarrow}$.

Temperature variation of photonic modes Ω^\uparrow and Ω^\downarrow

We assume that $\mu_\omega = 0$, $\mu_{\Omega^s} = 0.5$.

In Fig. 7(a), we chose four instances that vary in various μ_Ω : $\mu_\Omega^1 = 0$, $\mu_\Omega^2 = 0.1$, $\mu_\Omega^3 = 0.3$, $\mu_\Omega^4 = 0.5$. We discovered that neutral hydrogen molecule forms more quickly the higher the μ_Ω (or T_Ω). The circumstance where $\mu_\Omega^1 = 0$ (in this case, $T_\Omega^1 = 0K$) occurs is where formation moves the slowest, indicated by red solid curve. The fastest formation occurs when $\mu_\Omega^4 = 0.5$, indicated by green dashed-dotted curve. The probability of the $|\Psi_{final}\rangle$ never approaches 1 when the μ_Ω is equal to 0. However, once μ_Ω is bigger than 0, the probability of $|\Psi_{final}\rangle$ will reach 1 as long as the duration is long enough. Because molecule photons are not renewed, atomic photons are continually being added back into the system. Therefore, the entire system will progressively change in order to produce a stable molecular state.

We now raise μ_Ω from 0 to 0.5. In each case we take the value of final state when the number of iterations reaches 6000. We can intuitively perceive the trend of $|\Psi_{final}\rangle$ with the growth of μ_Ω in Fig. 7(b). Probability of $|\Psi_{final}\rangle$ is close to 0 when μ_Ω is near to 0. It begins to expand slowly as the μ_Ω rises, then quickly accelerates until it reaches a top, which is close to 1.

Temperature variation of photonic modes ω^\uparrow and ω^\downarrow

We assume that $\mu_\Omega = \mu_{\Omega^s} = 0.5$.

In Fig. 8(a), we chose four instances that vary in various μ_ω : $\mu_\omega^1 = 0$, $\mu_\omega^2 = 0.1$, $\mu_\omega^3 = 0.3$, $\mu_\omega^4 = 0.5$. And in Fig. 8(b) we increase μ_ω rises from 0 to 0.5.

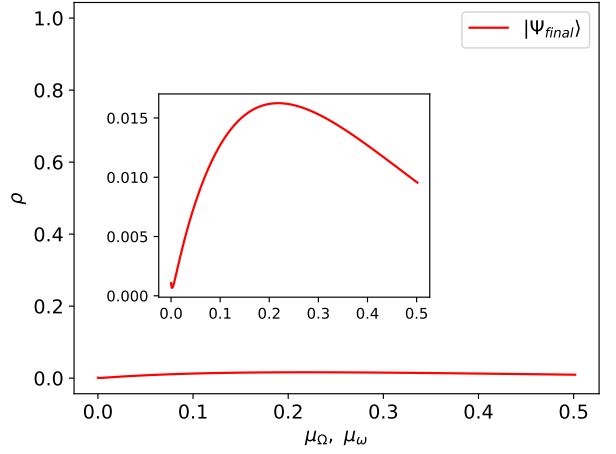


FIG. 9. (online color) *Counteraction of temperature variations of atomic and molecular photonic modes.* Red curve represents the probability of $|\Psi_{final}\rangle$ when iterations reaches 6000, with the simultaneous increases of μ_Ω and μ_ω from 0 to 0.5.

It is clear from Fig. 8 that the temperature variation of molecular photonic modes affects neutral evolution and hydrogen molecule formation in the opposite way from atomic photonic modes: the higher μ_ω (or T_ω), the slower evolution and formation.

The probability of the $|\Psi_{final}\rangle$ can reach 1 only when the μ_ω is 0, which is different from the Fig. 7(a). Even if the duration is long enough, when the μ_ω is not 0, the probability cannot increase to 1. The system will reach equilibrium between associative and dissociative systems because μ_Ω and μ_ω are both non-zero numbers at this point, meaning that the atomic and molecular photons are replenished simultaneously (although the replenishing efficiencies may differ). The value of the $|\Psi_{final}\rangle$ probability at equilibrium depends on the ratio of μ_Ω and μ_ω .

Counteraction of temperature variations of atomic and molecular photonic modes.

We said that temperature variation of atomic photonic modes is positive effect to evolution and formation of neutral hydrogen molecule, and temperature variation of molecular photonic modes is negative.

Now we consider these both opposite effects at the same time. We assume that $\mu_{\Omega^s} = 0.5$. And we increase μ_Ω , μ_ω both rises from 0 to 0.5. Specially, μ_Ω are always equal to μ_ω .

The probability of the $|\Psi_{final}\rangle$ curve in Fig. 9 is practically equal to zero as the atomic and molecular temperatures rise. Despite the curve's apparent small oscillation between the intervals [0, 0.016] in the inset graphic, we

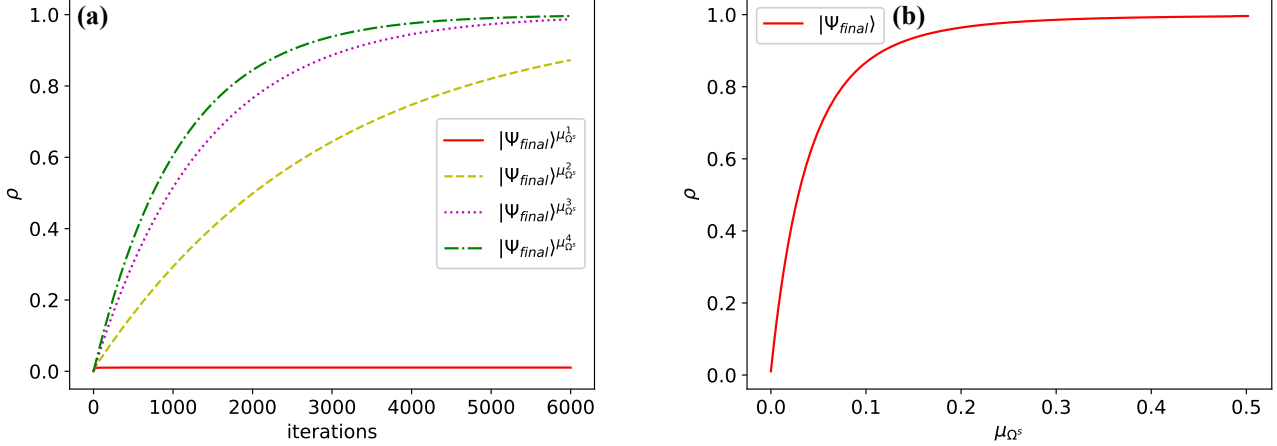


FIG. 10. (online color) Temperature variation of photonic mode Ω^s . In (a), time-dependent curves of $|\Psi_{final}\rangle$ are corresponding to $\mu_{\Omega^s}^1$ (red solid), $\mu_{\Omega^s}^2$ (yellow dashed), $\mu_{\Omega^s}^3$ (magenta dotted) and $\mu_{\Omega^s}^4$ (green dash-dotted), respectively. In (b), red curve represents the probability of $|\Psi_{final}\rangle$ when iterations reaches 6000, with the increases of μ_{Ω^s} from 0 to 0.5.

choose to ignore it. The initial state $|\Psi'_{initial}\rangle$, shown in Fig. 2(b), is not an equilibrium state between associative and dissociative systems, which accounts for the mild oscillations.

Thus, it is impossible for a neutral hydrogen molecule to form since the effects of temperature change on atomic and molecular photons cancel each other out.

Temperature variation of photonic modes Ω^s

We assume that $\mu_\omega = 0$, $\mu_\Omega = 0.5$.

In Fig. 10(a), we also chose four instances that vary in various μ_{Ω^s} : $\mu_{\Omega^s}^1 = 0$, $\mu_{\Omega^s}^2 = 0.1$, $\mu_{\Omega^s}^3 = 0.3$, $\mu_{\Omega^s}^4 = 0.5$. We found that the higher μ_{Ω^s} (or T_{Ω^s}), the faster formation of neutral hydrogen molecule. When $\mu_{\Omega^s}^1 = 0$ (here $T_{\Omega^s}^1 = 0K$), denoted by red solid curves, formation is slowest among all situations. When $\mu_{\Omega^s}^4 = 0.5$, denoted by green dash-dotted curves, formation is fastest among all situations. Same as μ_Ω , when the μ_{Ω^s} is equal to 0, the probability of $|\Psi_{final}\rangle$ never reaches 1. But once μ_{Ω^s} is greater than 0, then as long as the time is long enough, probability of $|\Psi_{final}\rangle$ will reach 1.

Now we increase μ_{Ω^s} from 0 to 0.5. In each case we take the value of final state when the number of iterations reaches 6000. In Fig. 10(b), when μ_{Ω^s} rises, probability of $|\Psi_{final}\rangle$ increases immediately abruptly. When μ_{Ω^s} is larger enough, probability of $|\Psi_{final}\rangle$ reaches top, which is close to 1.

D. With covalent bond and phonon

Now we introduce covalent bond and phonon in the association-dissociation model of neutral hydrogen

molecule. Initial state is $|\Psi''_{initial}\rangle$, described in Fig. 4.

According to numerical results in Fig. 11(a), we found red solid curve $|\Psi_{final}\rangle$ rises and reaches 1 at the end. And in Fig. 11(b), red solid curve $\{0 \succ_{cb}$ (as same as \mathcal{A}) also rises and reaches 1, and blue solid curve $\{1 \succ_{cb}$ (as same as \mathcal{D}) descends to 0. These results are consistent with Fig. 6. But this model is more straightforward and understandable.

VIII. CONCLUDING DISCUSSION AND FUTURE WORK

In this paper, we simulate the association of the neutral hydrogen molecule in the cavity QED model — the TCHM. The association-dissociation model has been constructed, and several analytical findings have been drawn from it:

In Secs. VII A and VII B, we proved hybridization of atomic orbitals and formation of neutral hydrogen molecule only happens when electrons with different spins. Then the influence of variation of T_{Ω^\uparrow} , T_{Ω^\downarrow} , T_{ω^\uparrow} , T_{ω^\downarrow} and T_{Ω^s} to the evolution and the formation of neutral hydrogen molecule is obtained in Sec. VII C: for $T_{\Omega^\uparrow}(T_{\Omega^\downarrow})$ and T_{Ω^s} , the higher temperature, the faster neutral hydrogen molecule formation; for $T_{\omega^\uparrow}(T_{\omega^\downarrow})$, the higher temperature, the slower neutral hydrogen molecule formation. Finally, we studied the more accurate model with covalent bond and phonon in Sec. VII D.

Although our approach is still imperfect, it has the advantages of being simple and scalable. It will be more subdued in this manner. Additionally, this model can be modified in the future for use with more intricate chemical and biologic models.

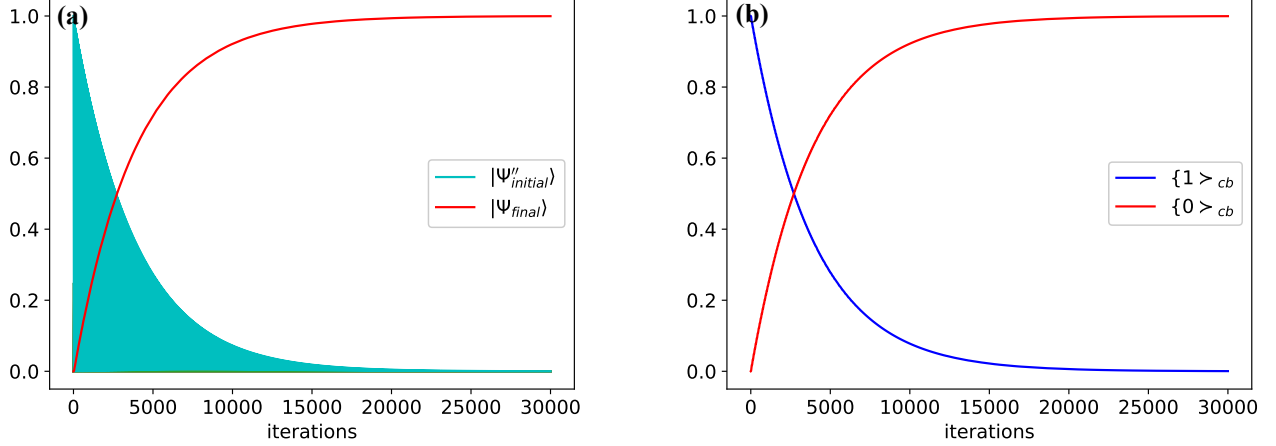


FIG. 11. (online color) *The evolution with consideration of covalent bond and phonon.* In (a), probability of state $|\Psi''_{initial}\rangle$ is denoted by cyan solid curve and probability of state $|\Psi_{final}\rangle$ is denoted by red solid curve. (b) shows the curves of time-dependent probabilities of $\{0 > cb\}$ and $\{1 > cb\}$. Probability of $\{0 > cb\}$ is denoted by red solid curve, and probability of $\{1 > cb\}$ is denoted by blue solid curve.

ACKNOWLEDGMENTS

This work was supported by the China Scholarship Council (CSC No.202108090483).

[1] Q. Wang, H.-Y. Liu, Q.-S. Li, Y. Li, Y. Chai, Q. Gong, H. Wang, Y.-C. Wu, Y.-J. Han, G.-C. Guo, and G.-P. Guo, Chemiq: A chemistry simulator for quantum computer (2021).

[2] J. R. McClean, N. C. Rubin, J. Lee, M. P. Harrigan, T. E. O'Brien, R. Babbush, W. J. Huggins, and H.-Y. Huang, What the foundations of quantum computer science teach us about chemistry, *The Journal of Chemical Physics* **155**, 150901 (2021).

[3] D. Claudino, A. J. McCaskey, and D. I. Lyakh, A backend-agnostic, quantum-classical framework for simulations of chemistry in C++, *ACM Transactions on Quantum Computing* 10.1145/3523285 (2022), just Accepted.

[4] J. Zhu, Quantum simulation of dissociative ionization of h_2^+ in full dimensionality with a time-dependent surface-flux method, *Phys. Rev. A* **102**, 053109 (2020).

[5] A. Vitaliy, K. Zheng, K. Alexei, H. Miao, O. Yuri, L. Wanshun, and V. Nadezda, About chemical modifications of finite dimensional qed models, *Nonlinear Phenomena in Complex Systems* **24**, 230 (2021).

[6] C. Ran, Y. Ozhigov, and Y. Jiangchuan, Qualitative model of a positive hydrogen peroxide ion in a thermal bath, arXiv preprint arXiv:2212.10662 (2022).

[7] S. Haroche, Nobel lecture: Controlling photons in a box and exploring the quantum to classical boundary, *Rev. Mod. Phys.* **85**, 1083 (2013).

[8] X. Gu, A. F. Kockum, A. Miranowicz, Y. xi Liu, and F. Nori, Microwave photonics with superconducting quantum circuits, *Physics Reports* **718-719**, 1 (2017), microwave photonics with superconducting quantum circuits.

[9] A. F. Kockum and F. Nori, Quantum bits with josephson junctions, in *Fundamentals and Frontiers of the Josephson Effect*, edited by F. Tafuri (Springer International Publishing, Cham, 2019) pp. 703–741.

[10] A. Frisk Kockum, A. Miranowicz, S. De Liberato, S. Savasta, and F. Nori, Ultrastrong coupling between light and matter, *Nature Reviews Physics* **1**, 19 (2019).

[11] P. Forn-Díaz, L. Lamata, E. Rico, J. Kono, and E. Solano, Ultrastrong coupling regimes of light-matter interaction, *Rev. Mod. Phys.* **91**, 025005 (2019).

[12] I. I. Rabi, On the process of space quantization, *Phys. Rev.* **49**, 324 (1936).

[13] I. I. Rabi, Space quantization in a gyrating magnetic field, *Phys. Rev.* **51**, 652 (1937).

[14] R. H. Dicke, Coherence in spontaneous radiation processes, *Phys. Rev.* **93**, 99 (1954).

[15] J. J. Hopfield, Theory of the contribution of excitons to the complex dielectric constant of crystals, *Phys. Rev.* **112**, 1555 (1958).

[16] J. Casanova, G. Romero, I. Lizuain, J. J. García-Ripoll, and E. Solano, Deep strong coupling regime of the jaynes-cummings model, *Phys. Rev. Lett.* **105**, 263603 (2010).

[17] E. Jaynes and F. Cummings, Comparison of quantum and semiclassical radiation theories with application to the beam maser, *Proceedings of the IEEE* **51**, 89 (1963).

[18] M. Tavis and F. W. Cummings, Exact solution for an n -

molecule—radiation-field hamiltonian, Phys. Rev. **170**, 379 (1968).

[19] D. G. Angelakis, M. F. Santos, and S. Bose, Photon-blockade-induced mott transitions and xy spin models in coupled cavity arrays, Phys. Rev. A **76**, 031805 (2007).

[20] H. Wei, J. Zhang, S. Greschner, T. C. Scott, and W. Zhang, Quantum monte carlo study of superradiant supersolid of light in the extended jaynes-cummings-hubbard model, Phys. Rev. B **103**, 184501 (2021).

[21] S. Prasad and A. Martin, Effective three-body interactions in jaynes-cummings-hubbard systems, Sci Rep **8**, 16253 (2018).

[22] L. Guo, S. Greschner, S. Zhu, and W. Zhang, Supersolid and pair correlations of the extended jaynes-cummings-hubbard model on triangular lattices, Phys. Rev. A **100**, 033614 (2019).

[23] K. C. Smith, A. Bhattacharya, and D. J. Masiello, Exact k -body representation of the jaynes-cummings interaction in the dressed basis: Insight into many-body phenomena with light, Phys. Rev. A **104**, 013707 (2021).

[24] A. Kulagin and Y. Ozhigov, Realization of grover search algorithm on the optical cavities, Lobachevskii J Math **43**, 864 (2022).

[25] Y. Ozhigov, Quantum gates on asynchronous atomic excitations, Quantum Electron. **50**, 10.1070/QUE17320 (2020).

[26] R. Düll, A. Kulagin, W. Lee, Y. Ozhigov, H. Miao, and K. Zheng, Quality of control in the tavis-cummings-hubbard model, Computational Mathematics and Modeling **32**, 75 (2021).

[27] Y. I. Ozhigov, Space of dark states in tavis-cummings model, Modern Information Technologies and IT Education **15**, 27 (2019).

[28] A. V. Kulagin and Y. I. Ozhigov, Optical selection of dark states of multilevel atomic ensembles, Computational Mathematics and Modeling **31**, 431 (2020).

[29] V. Afanasyev, C. Ran, Y. Ozhigov, and Y. Jiangchuan, Collapse of dark states in tavis-cummings model, arXiv preprint arXiv:2207.03175 (2022).

[30] N. Victorova, A. Kulagin, and Y. Ozhigov, Quasiclassical description of the “quantum bottleneck” effect for thermal relaxation of an atom in a resonator, Comput Math Model **31**, 1 (2020).

[31] Y. Ozhigov, About quantum computer software, Quantum Information and Computation **20**, 570 (2020).

[32] Y. Ozhigov and I. Pluzhnikov, Superimposition and antagonism in chain synthesis using entangled biphotonic control, Comput Math Model **33**, 24 (2022).

[33] Y. Ozhigov, Three principles of quantum computing, Quantum Information and Computation **22**, 1280 (2022).

[34] H.-P. Breuer, F. Petruccione, *et al.*, *The theory of open quantum systems* (Oxford University Press, 2002).

[35] R. Alicki, The quantum open system as a model of the heat engine, Journal of Physics A: Mathematical and General **12**, L103 (1979).

[36] R. Kosloff, Quantum thermodynamics: A dynamical viewpoint, Entropy **15**, 2100 (2013).

[37] W. Pauli, Über den Zusammenhang des Abschlusses der Elektronengruppen im Atom mit der Komplexstruktur der Spektren, Zeitschrift für Physik **31**, 765 (1925).

[38] P. A. M. Dirac, The quantum theory of the emission and absorption of radiation, Proc. R. Soc. A, 243 (1927).

[39] V. Fock, Konfigurationsraum und zweite quantelung, Zeitschrift für Physik **75**, 622 (1932).

[40] Y. Wu and X. Yang, Strong-coupling theory of periodically driven two-level systems, Phys. Rev. Lett. **98**, 013601 (2007).

[41] A. Kulagin, V. Ladunov, Y. Ozhigov, N. Skovoroda, and N. Victorova, Homogeneous atomic ensembles and single-mode field: review of simulation results, in *International Conference on Micro-and Nano-Electronics 2018*, Vol. 11022 (SPIE, 2019) pp. 600–611.

[42] G. Rempe, H. Walther, and N. Klein, Observation of quantum collapse and revival in a one-atom maser, Phys. Rev. Lett. **58**, 353 (1987).

Appendix A: Complete expressions for TCHM

1. TCM

We consider the TCM to describe the interaction of atomic ensembles (N atoms) with photons in an optical cavity (the simplest model with a two-level atom, called JCM, is shown in Fig. 12(a)). Hamiltonian of TCM for the weak interaction $g \ll \hbar\omega_c \approx \hbar\omega_a$ (RWA) looks as follows

$$H_{TC} = \underbrace{\hbar\omega_c a^\dagger a}_{H_{field}} + \underbrace{\hbar\omega_a \sum_{i=1}^N \sigma_i^\dagger \sigma_i}_{H_{atoms}} + \underbrace{\sum_{i=1}^N g_i (a^\dagger + a)(\sigma_i^\dagger + \sigma_i)}_{H_{int}} \quad (A1a)$$

$$H_{TC}^{RWA} = \hbar\omega_c a^\dagger a + \hbar\omega_a \sum_{i=1}^N \sigma_i^\dagger \sigma_i + \sum_{i=1}^N g_i (a^\dagger \sigma_i + a \sigma_i^\dagger) \quad (A1b)$$

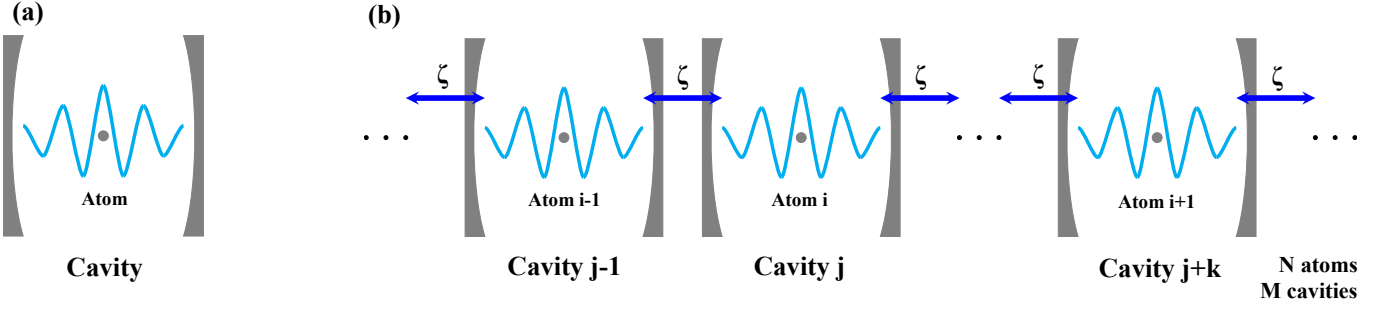


FIG. 12. (online color) *TCM and TCHM*. TCM with a two-level atom in an optical cavity is shown in (a), TCHM with N two-level atoms and M optical cavities coupled by an optical fibre is shown in (b). Atoms are denoted by gray dots.

where operators a , a^\dagger are written as follows

$$a = \begin{pmatrix} |0\rangle & |1\rangle & |2\rangle & \cdots & \cdots & |p-2\rangle & |p-1\rangle & |p\rangle \\ |0\rangle & 0 & 1 & 0 & \cdots & \cdots & 0 & 0 & 0 \\ |1\rangle & 0 & 0 & \sqrt{2} & \cdots & \cdots & 0 & 0 & 0 \\ |2\rangle & 0 & 0 & 0 & \ddots & & 0 & 0 & 0 \\ \vdots & \vdots & \vdots & \ddots & \ddots & \ddots & \vdots & \vdots & \vdots \\ \vdots & \vdots & \vdots & \ddots & \ddots & \ddots & \vdots & \vdots & \vdots \\ |p-2\rangle & 0 & 0 & 0 & \cdots & \cdots & 0 & \sqrt{m-1} & 0 \\ |p-1\rangle & 0 & 0 & 0 & \cdots & \cdots & 0 & 0 & \sqrt{m} \\ |p\rangle & 0 & 0 & 0 & \cdots & \cdots & 0 & 0 & 0 \end{pmatrix} \quad (A2)$$

$$a^\dagger = \begin{pmatrix} |0\rangle & |1\rangle & |2\rangle & \cdots & \cdots & |p-2\rangle & |p-1\rangle & |p\rangle \\ |0\rangle & 0 & 0 & 0 & \cdots & \cdots & 0 & 0 & 0 \\ |1\rangle & 1 & 0 & 0 & \cdots & \cdots & 0 & 0 & 0 \\ |2\rangle & 0 & \sqrt{2} & 0 & \ddots & & 0 & 0 & 0 \\ \vdots & \vdots & \vdots & \ddots & \ddots & \ddots & \vdots & \vdots & \vdots \\ \vdots & \vdots & \vdots & \ddots & \ddots & \ddots & \vdots & \vdots & \vdots \\ |p-2\rangle & 0 & 0 & 0 & \cdots & \ddots & 0 & 0 & 0 \\ |p-1\rangle & 0 & 0 & 0 & \cdots & \cdots & \sqrt{m-1} & 0 & 0 \\ |p\rangle & 0 & 0 & 0 & \cdots & \cdots & 0 & \sqrt{m} & 0 \end{pmatrix} \quad (A3)$$

where $|p\rangle$ corresponds to the number of photons in an optical cavity. For two-level atoms, operators σ , σ^\dagger are written as follows

$$\sigma = \begin{pmatrix} |0\rangle & |1\rangle \\ |0\rangle & \begin{pmatrix} 0 & 1 \\ 0 & 0 \end{pmatrix} \end{pmatrix} \quad (A4)$$

$$\sigma^\dagger = \begin{pmatrix} |0\rangle & |1\rangle \\ |0\rangle & \begin{pmatrix} 0 & 0 \\ 1 & 0 \end{pmatrix} \end{pmatrix} \quad (A5)$$

where $|0\rangle$ — ground state, $|1\rangle$ — excited state.

2. TCHM

TCM has been generalized to several cavities coupled by an optical fibre — TCHM in Fig. 12(b). Photons can move between optical cavities through optical fibres. Hamiltonian of TCHM for RWA looks as follows

$$H_{TCH} = \sum_{j=1}^M \left(\underbrace{\hbar\omega_{c_j} a_j^\dagger a_j + \hbar\omega_{a_j} \sum_{i=1}^N \sigma_{i,j}^\dagger \sigma_{i,j} + \sum_{i=1}^N g_i (a_j^\dagger + a_j)(\sigma_{i,j}^\dagger + \sigma_{i,j})}_{H_{TC}} \right) + \zeta \sum_{j=1}^M (a_{j+1}^\dagger a_j + a_j^\dagger a_{j+1}) \quad (\text{A6a})$$

$$H_{TCH}^{RWA} = \sum_{j=1}^M \left(\hbar\omega_{c_j} a_j^\dagger a_j + \hbar\omega_{a_j} \sum_{i=1}^N \sigma_{i,j}^\dagger \sigma_{i,j} + \sum_{i=1}^N g_i (a_j^\dagger \sigma_{i,j} + a_j \sigma_{i,j}^\dagger) \right) + \zeta \sum_{j=1}^M (a_{j+1}^\dagger a_j + a_j^\dagger a_{j+1}) \quad (\text{A6b})$$

where M — number of optical cavities, ζ — atoms leap strength (tunnelling strength) between neighbouring cavities.

Appendix B: Theorem for thermally stationary state

Theorem Thermally stationary state of atoms and field at the temperature T has the form

$$\rho_{stat} = \rho_{ph} \otimes \rho_{at} \quad (\text{B1})$$

where ρ_{at} is the state of atoms and the state of field $\rho_{ph} = \mathcal{G}(T)_f$ is equilibrium state at this temperature.

Proof We expand Hamiltonian $H = H_{at} + H_{ph}$ to the atomic part H_{at} and purely photonic component $H_{ph} = \hbar\omega a^\dagger a$, and introduce notations $U_{dt}(\rho) = e^{-\frac{i}{\hbar} H_{at} dt} \rho e^{\frac{i}{\hbar} H_{at} dt}$, $U'_{dt}(\rho) = e^{-\frac{i}{\hbar} H_{ph} dt} \rho e^{\frac{i}{\hbar} H_{ph} dt}$ for the action of summands of the unitary part of the Lindblad superoperator \mathcal{L} in Eq. (5) to the density matrix on the short time segment dt .

We denote through $L'_{dt}(\rho) = \rho + idtL(\rho)$ the action of Lindblad superoperator on the density matrix in the time dt . With accuracy dt we then have the approximate equation

$$\rho(t) \approx (U_{dt} U'_{dt} L'_{dt})^{\frac{t}{dt}}(\rho) \quad (\text{B2})$$

analogous to the Trotter formula, which comes from Euler method of the solution of quantum master equation in Eq. (5).

Since operators L'_{dt} , U'_{dt} act on the photon component of state only, and U_{dt} — on the photon and atomic components, the stationary state ρ_{stat} at the randomly chosen constants of interaction g , $\gamma_{k'}$, γ_k must not change after the action of operators a $L''_{dt} = U'_{dt} L'_{dt}$, and operator U_{dt} .

We fix arbitrary basic state of atoms I , J and consider the minor ρ_{IJ} of the matrix ρ , formed by coefficients at the basic states $|I, i\rangle\langle J, j|$, where $|i\rangle$, $|j\rangle$ — are Fock state of the field. The operator L'_{dt} , acting on the photon states, factually acts on the minor ρ_{IJ} .

We will denote by the sign $\tilde{\rho}$ the result of the application of operator L'_{dt} to the minor $\rho_{IJ} = \rho$, so that $\tilde{\rho}_{ij}$ denote matrix elements of this result and ρ_{ij} — matrix elements of the initial state ρ ; we will enumerate rows and columns of this matrix beginning with zero, so that $i, j = 0, 1, 2, \dots$, and omit in the notation atomic states I, J , which will always be the same. Taking into account the definition of operators of the creation and annihilation of photons, we have

$$\tilde{\rho}_{ij} = \rho_{ij} + \gamma_k (\sqrt{i+1} \sqrt{j+1} \rho_{i+1, j+1} - \frac{i+j}{2} \rho_{ij}) + \gamma_{k'} (\sqrt{i} \sqrt{j} \rho_{i-1, j-1} - (\frac{i+j}{2} + 1) \rho_{ij}) \quad (\text{B3})$$

We also have $L''_{dt}(\rho) = \rho$, $L''_{dt}(\tilde{\rho}) = \tilde{\rho}$. The operator U'_{dt} does not change the diagonal members of the matrix, and it multiplies nondiagonal members to the coefficient $e^{\pm i\omega(i-j)dt}$. Because the coefficient ω , determining the phase is not connected with $\gamma_{k'}$ and γ_k from the Eq. (B3), this multiplication cannot compensate in the first order on dt the addition to ρ_{ij} from Eq. (B3), and hence in the matrix ρ nondiagonal members are zero. We consider the diagonal of this matrix. From the Eq. (B3) we have

$$\tilde{\rho}_{ii} = \rho_{ii} + \gamma_k ((i+1) \rho_{i+1, i+1} - i \rho_{ii}) + \gamma_{k'} (i \rho_{i-1, i-1} - (i+1) \rho_{ii}) \quad (\text{B4})$$

From the Eq. (B4) we can obtain the recurrent equation for the elements of diagonal, but it is possible to get their form easier. We apply to the diagonal of ρ the representation of quantum hydrodynamics. The flow of probability from the basic state $|i\rangle\langle i|$ to the state $|i+1\rangle\langle i+1|$ is $(i+1)\rho_{ii}\gamma_{k'}$, and the reverse flow is $(i+1)\rho_{i+1,i+1}\gamma_k$, from which we get that ρ_{ii} is proportional to μ^i , that is required.

Now we substitute this expression for the diagonal element to the Eq. (B4), and obtain $\tilde{\rho}_{ii} = \rho_{ii}$. Since the choice of I , J was arbitrary, we obtain $\rho_{stat} = \mathcal{G}(T)_f \otimes \rho_{at}$, that is required. Theorem is proved.

Appendix C: Tensor product and generator algorithm

Now we consider the simplest TCM with only one two-level atom, which is shown in Fig. 12(a). And its Hamiltonian with RWA takes following form

$$\begin{aligned}
H_{TC}^{RWA} &= \hbar\omega a^\dagger a + \hbar\omega\sigma^\dagger\sigma + g(a^\dagger\sigma + a\sigma^\dagger) \\
&= \hbar\omega a^\dagger a \otimes I_\sigma + I_a \otimes \hbar\omega\sigma^\dagger\sigma + g[(a^\dagger \otimes I_\sigma)(I_a \otimes \sigma) + (a \otimes I_\sigma)(I_a \otimes \sigma^\dagger)] \\
&= \hbar\omega \begin{pmatrix} |0\rangle & |1\rangle \\ |1\rangle & |0\rangle \end{pmatrix}_{ph} \otimes \begin{pmatrix} |0\rangle & |1\rangle \\ |1\rangle & |0\rangle \end{pmatrix}_{at} + \hbar\omega \begin{pmatrix} |0\rangle & |1\rangle \\ |1\rangle & |0\rangle \end{pmatrix}_{ph} \otimes \begin{pmatrix} |0\rangle & |1\rangle \\ |1\rangle & |0\rangle \end{pmatrix}_{at} \\
&\quad + g \left[\left(\begin{pmatrix} |0\rangle & |1\rangle \\ |1\rangle & |0\rangle \end{pmatrix}_{ph} \otimes \begin{pmatrix} |0\rangle & |1\rangle \\ |1\rangle & |0\rangle \end{pmatrix}_{at} \right) \left(\begin{pmatrix} |0\rangle & |1\rangle \\ |1\rangle & |0\rangle \end{pmatrix}_{ph} \otimes \begin{pmatrix} |0\rangle & |1\rangle \\ |1\rangle & |0\rangle \end{pmatrix}_{at} \right) \right. \\
&\quad \left. + \left(\begin{pmatrix} |0\rangle & |1\rangle \\ |1\rangle & |0\rangle \end{pmatrix}_{ph} \otimes \begin{pmatrix} |0\rangle & |1\rangle \\ |1\rangle & |0\rangle \end{pmatrix}_{at} \right) \left(\begin{pmatrix} |0\rangle & |1\rangle \\ |1\rangle & |0\rangle \end{pmatrix}_{ph} \otimes \begin{pmatrix} |0\rangle & |1\rangle \\ |1\rangle & |0\rangle \end{pmatrix}_{at} \right) \right] \\
&= \begin{pmatrix} |0\rangle|0\rangle & |0\rangle|1\rangle & |1\rangle|0\rangle & |1\rangle|1\rangle \\ |0\rangle|0\rangle & 0 & 0 & 0 \\ |0\rangle|1\rangle & 0 & \hbar\omega & g \\ |1\rangle|0\rangle & 0 & g & \hbar\omega \\ |1\rangle|1\rangle & 0 & 0 & 2\hbar\omega \end{pmatrix}_{ph \otimes at} \tag{C1}
\end{aligned}$$

where I_a , I_σ are unit operators, $\omega = \omega_c = \omega_a$. Via tensor product (shown in Fig. 13(a)) we create a 4 by 4 matrix. Now we assume that initial state is $|0\rangle|1\rangle$ and dissipation of photon is allowed, thus we only have three states $|0\rangle|0\rangle$, $|1\rangle|0\rangle$, $|0\rangle|1\rangle$ in the system. $|1\rangle|1\rangle$ doesn't exist according to the initial state. It is useless. Hamiltonian is rewritten as

$$H_{TC}^{RWA} = \begin{pmatrix} |0\rangle|0\rangle & |0\rangle|1\rangle & |1\rangle|0\rangle \\ |0\rangle|0\rangle & 0 & 0 \\ |0\rangle|1\rangle & 0 & \hbar\omega \\ |1\rangle|0\rangle & 0 & g \\ |1\rangle|1\rangle & 0 & 0 \end{pmatrix}_{ph \otimes at} \tag{C2}$$

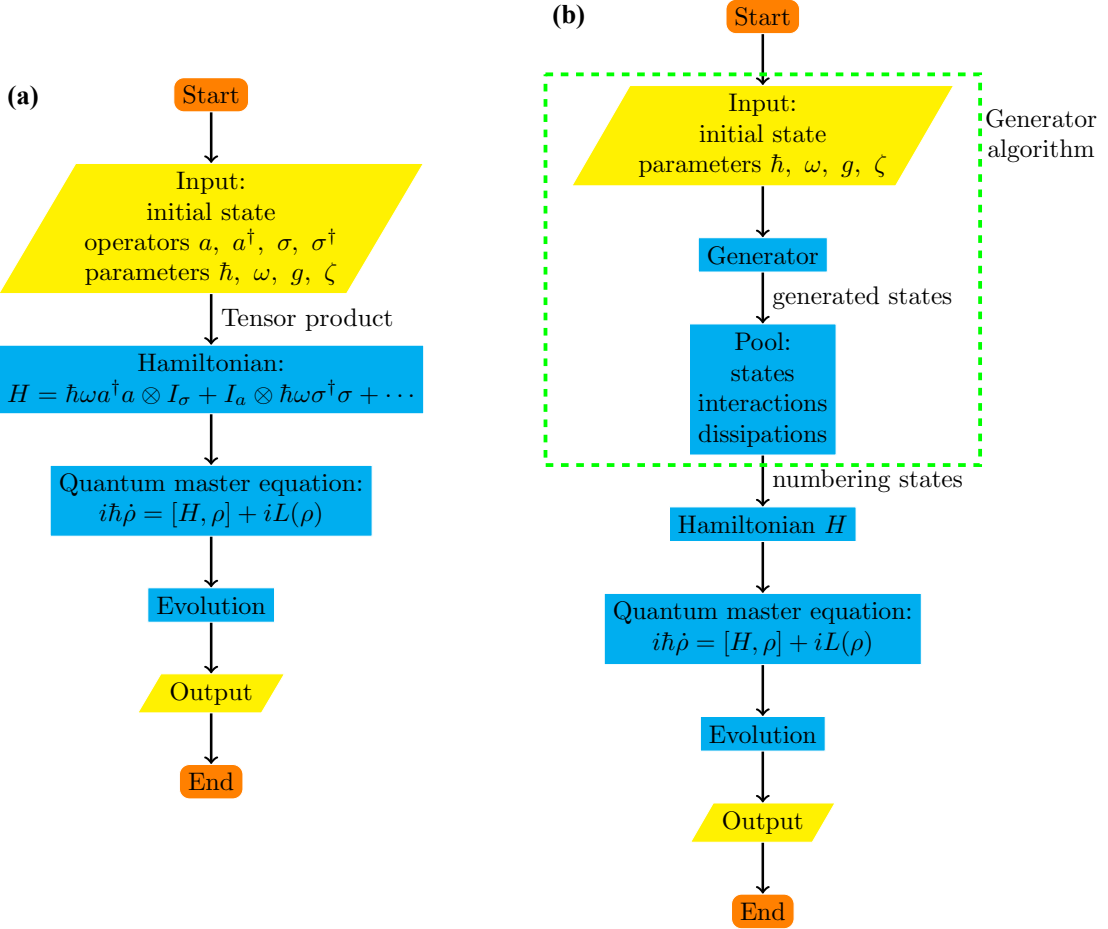
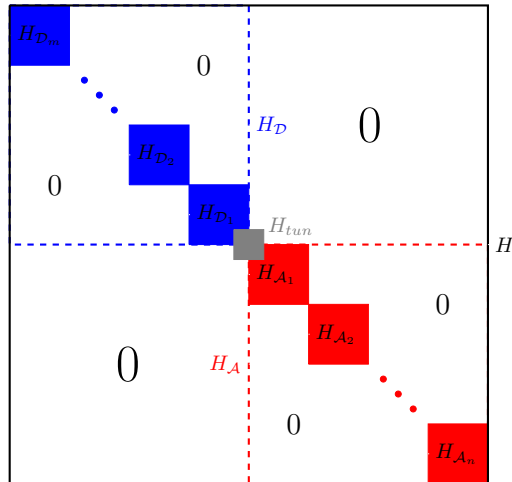
Now the new Hamiltonian is 3 by 3. If closed system is considered, then dissipation is forbidden. $|0\rangle|0\rangle$ is also useless. Hamiltonian is as follows

$$H_{TC}^{RWA} = \begin{pmatrix} |0\rangle|1\rangle & |1\rangle|0\rangle \\ |0\rangle|1\rangle & \hbar\omega & g \\ |1\rangle|0\rangle & g & \hbar\omega \end{pmatrix}_{ph \otimes at} \tag{C3}$$

Now the new Hamiltonian is 2 by 2.

Tensor product is actually a common but ineffective method of producing a full Hamiltonian. We typically do not require the complete Hamiltonian due to initial condition restrictions. The relevant portion frequently only takes up a very small portion of the Hilbert space, particularly for complex multi-particle systems. In order to throw away extraneous unneeded states while maintaining beneficial states, we add the generator method depicted in Fig. 13(b). The core is establishing Hamiltonian with states generated by generator algorithm according to initial state and possible interactions and dissipations among them.

The fact that the generator approach doesn't require an operator is the main distinction between it and the tensor product algorithm. As a result, we are free to assign any number to each state when breaking up the Hamiltonian. For instance, the association-dissociation Hamiltonian of the neutral hydrogen molecule, described in Eq. (9), is divided similarly in this article as seen in Fig. 14.

FIG. 13. (online color) *Tensor product and generator algorithm.*FIG. 14. (online color) *Hamiltonian of the association-dissociation of neutral hydrogen molecule. $H = H_D + H_A + H_{tun} = \sum_i^m H_{D_i} + \sum_j^n H_{A_j} + H_{tun}$.*